

Protracted Vascular Retinopathy in a Novel Model of Spontaneous Type 2 Diabetes

by

Jonathan Gotzmann

A thesis submitted in partial fulfillment of the requirements for the degree of

Master of Science

Department of Physiology

University of Alberta

© Jonathan Gotzmann, 2015

Abstract

Diabetic retinopathy (DR) is the leading cause of blindness in working aged adults, however lack of a suitable animal model has limited our understanding of the disease. The Nile grass rat (NR) is a cone-rich crepuscular rodent that spontaneously develops hyperglycemia (HG) when fed standard lab chow, making them a candidate to study the effects of HG on the retina. Vascular integrity was assessed in two groups of NRs at 6, 12 and 18 months of age: 1) standard lab chow: fed Prolab 2000 (HG); 2) low calorie, high fiber diet: fed Mazuri Chinchilla (control). Results revealed many classic hallmarks of human DR, such as pericyte loss, degeneration of capillaries and microaneurysm formation. Furthermore, early cataract development was seen in hyperglycemic NRs, as early as 12 months of age. In addition to the classic vascular changes associated with DR, differences in inner retinal circuitry were investigated. Hyperglycemic NRs showed a decreased ability for age-related dendritic sprouting specific to dopaminergic amacrine cells and also a marked reduction of connexin 36 (Cx36) expression in the outer plexiform layer (OPL) and inner plexiform layer (IPL). Together, our results demonstrate that NRs recapitulate the key pathological features and slow time course of early human DR. Therefore, NRs provide a unique opportunity to study the pathogenesis of DR as well as providing new understanding to the changes of the diabetic retina.

Acknowledgments

I have immense gratitude for the opportunity I have had to study under the supervision of Dr. Yves Sauvé. My project would not have been possible without his commitment to training me both technically and intellectually. His passion and devotion to research has inspired me to continually grow as a researcher. I would also like to thank my committee members, Dr. Ted Allison and Dr. Cathy Chan for their guidance and support throughout my graduate studies both academically and personally.

I owe many thanks to all the members of the Sauvé lab: Emma Stephens, Rachel Bryant, Camille Dejos and Sharee Kuny. Specifically, I would like to acknowledge Sharee for her guidance on planning and carry out experiments, in addition to the numerous hours spent working with me in the lab. I would also like to thank Gordon Hagerman for his guidance in choosing appropriate statistical tests.

Finally, I would like to thank Dr. John Dimopoulos for his intellectual contribution, advice and friendship. His clinical insights have helped me understand the bigger picture, as well as inspiring me to pursue a career as a clinical scientist.

All the work reported in this thesis was conducted with the financial support of the following funding agencies: Alberta diabetes institute (ADI) and Canadian Institutes of Health Research (CIHR).

Table of Contents

LIST OF TABLES.....	VII
LIST OF FIGURES.....	VIII
LIST OF ABBREVIATIONS.....	X
CHAPTER. 1 INTRODUCTION.....	1
1.1) DIABETES MELLITUS.....	1
1.2) DIABETIC RETINOPATHY.....	4
1.3) RETINAL MICROVASCULATURE.....	7
1.4) CELLULAR MECHANISM OF DIABETIC RETINOPATHY.....	9
1.5) CURRENT ANIMAL MODELS OF DIABETIC RETINOPATHY.....	11
1.6) NILE GRASS RAT BACKGROUND.....	14
1.7) FUNDUS IMAGING.....	15
1.8) ELECTRORETINOGRAM.....	16
1.9) THE ELECTRORETINOGRAM IN DIABETIC RETINOPATHY.....	18
CHAPTER. 2 RESEARCH PLAN.....	20
2.1) RATIONALE.....	20
2.2) HYPOTHESIS.....	21
2.3) OBJECTIVES.....	22
CHAPTER. 3 EXPERIMENTAL DESIGN AND METHODS.....	23
3.1) EXPERIMENTAL DESIGN.....	23
3.1A) Animals.....	23
3.2B) Dietary Manipulation.....	23
3.2 TISSUE COLLECTION.....	25
3.2A) Blood Collection.....	25

3.2B) Ocular Tissue Collection	26
3.2C) Supplementary Tissue Collection	27
3.3) EXPERIMENTAL METHODS	29
3.3A) Whole Body Composition	29
3.3B) Fasted blood glucose.....	30
3.3C) Glycated Hemoglobin	30
3.3D) Plasma Insulin.....	32
3.3E) Retinal Digests	32
3.3F) Fluorescein Angiography	34
3.4) IMMUNOHISTOCHEMISTRY	35
3.4A) Cross-sections	35
3.4B) Retinal Flat Mount	37
3.5) ELECTRORETINOGRAM.....	38
3.6) STATISTICAL ANALYSIS	39
3.7) SUBJECTS.....	40
CHAPTER. 4 RESULTS.....	40
4.1) METABOLIC PHENOTYPE.....	40
4.1A) Dietary effect on fasted blood glucose	40
4.1B) Dietary effect on glycated hemoglobin.....	43
4.1C) Dietary effect on plasma insulin	44
4.1D) Dietary effect on bodyweight	44
4.1E) Dietary manipulation of glycemic status	46
4.2) RETINAL VASCULAR ANALYSIS.....	46
4.2A) Isolated vascular integrity.....	46
4.2B) In vivo vascular integrity	50

4.3) RETINA CROSS-SECTIONAL STAINING	53
4.3A) Amacrine cells	53
4.3B) Connexin 36	59
4.3C) Connexin 43	60
4.3D) Glial Fibrillary Acidic Protein	61
4.3E) Tomato Lectin	62
4.3F) Retinal Flat Mount	63
4.4) ELECTRORETINOGRAM.....	64
4.4A) Anesthesia.....	64
4.4B) Comparison between human and Nile rat oscillatory potentials	65
CHAPTER. 5 DISCUSSION	68
5.1) GLYCEMIC STATUS.....	68
5.2) EFFECT OF HYPERGLYCEMIA ON THE RETINA	71
5.2A) Pericyte loss	71
5.2B) In-vivo vascular integrity.....	75
5.2C) Age-related dendritic sprouting	77
5.2D) Delayed dark-adaptation in diabetic retinopathy	78
5.3) SUMMARY	79
5.4) FUTURE DIRECTIONS.....	79
5.5) CONCLUSION	81
REFERENCES	83

List of Tables

Table 1: Nutritional composition of the Mazuri chinchilla and Prolab 2000 diet 25

Table 2: Echo MRI Analyses 46

List of Figures

Figure 1.1: Schema representing the progression of T2DM.....	3
Figure 1.2: Relative risk of developing microvascular complications	4
Figure 1.3: Diabetic retinopathy clinically detectable features	5
Figure 1.4: Pericyte/endothelial cell structural and functional roles	9
Figure 1.5: Flow diagram of the proposed key factors involved in the pathogenesis of diabetic retinopathy and associated clinical signs	11
Figure 1.6: Fundus imaging of a healthy and diabetic retina.....	16
Figure 1.7: Amplitude and implicit time measurements of the ERG waveform	17
Figure 1.8: Components and origin of the ERG waveforms	18
Figure 3.1: Retinal cross-section measurements.....	37
Figure 4.1: Effect of diet and age on fasted blood glucose levels	42
Figure 4.2: Effect of diet and age on glycated hemoglobin levels.....	43
Figure 4.3: Effect of diet and age on bodyweight.....	45
Figure 4.4: Retinal digest preparations of control and HG retinas	49
Figure 4.5: Progressive cataract development in hyperglycemic NRs	51
Figure 4.6: Example of a capillary microaneurysm.....	51
Figure 4.7: Representative fluorescein angiography fundus images	52
Figure 4.8: Cross-sectional analysis of cholinergic amacrine cells	56
Figure 4.9: Cross-sectional analysis of dopaminergic amacrine cells	59
Figure 4.10: Effect of hyperglycemia on Cx36 expression	60
Figure 4.11: Effect of hyperglycemia on Cx43 expression	61
Figure 4.12: Effect of hyperglycemia on GFAP expression.....	62

Figure 4.13: Effect of hyperglycemia on inner retinal vasculature morphology	62
Figure 4.14: Example of retinal flat-mount stained with anti-TH	64
Figure 4.15: Comparison of filtered human and NR ON-OPs.....	67
Figure 5.1: Proposed mechanism of hypoxia-induced pericyte loss.....	75

List of Abbreviations

Ab - Antibody

AFB – American Foundation for the Blind

AGE – Advanced glycation end-product

Ang1 – Angiotensin 1

Ang2 – Angiotensin 2

ANOVA – Analysis of variance

ARVO – The Association for Research in Vision and Ophthalmology

BMI – Body mass index

ChAT – Choline acetyl transferase

CNS – Central nervous system

Cx36 – Connexin 36

Cx43 – Connexin 43

DM – Diabetes mellitus

DR – Diabetic retinopathy

EC – Endothelial cell

EDTA – Ethylenediaminetetraacetic acid

ERG - Electroretinogram

FA – Fluorescein angiography

FBG – Fasted blood glucose

GCL – Ganglion cell layer

GFAP – Glial fibrillary acidic protein

GHb – Glycated hemoglobin

HG - hyperglycemia

HIF – Hypoxic inducing factor

ICAM – Intercellular adhesion molecule

IP – Intra-peritoneal

IPL – Inner plexiform layer

K - Potassium

Mets – Metabolic syndrome

MMP – Matrix metalloproteinase

MO – microvascular occlusion

MRI – Magnetic resonance imaging

Na - Sodium

NEI – National Eye Institute

NMR – Nuclear magnetic resonance

Non-GHb – Non-glycated hemoglobin

NPDR – non-proliferative diabetic retinopathy

NR – Nile grass rat

OP – Oscillatory potential

OPL – Outer plexiform layer

P:EC – Pericyte-to-endothelial cell

PAS – Periodic acid Schiff

PBS – Phosphate buffered saline

PDGF – Platelet derived growth factor

PDR – Proliferative diabetic retinopathy

PFA - Paraformaldehyde

PKC Protein kinase C

RBC – Red blood cell

STZ - Streptozotocin

T1DM – Type 1 diabetes mellitus

T2DM – Type 2 diabetes mellitus

TGF – Transforming growth factor

TH – Tyrosine hydroxylase

TIMP – Tissue inhibitor of metalloproteinase

UKPDS – The United Kingdom Prospective Diabetes Study

VEGF – Vascular endothelial growth factor

Chapter. 1 INTRODUCTION

1.1) Diabetes Mellitus

Diabetes Mellitus (DM) is a metabolic disorder characterized by chronic hyperglycemia (HG), stemming from decreased insulin production and/or sensitivity to insulin. DM is commonly categorized into two types: type 1 diabetes mellitus (T1DM) and type 2 diabetes mellitus (T2DM). T1DM is often referred to as insulin-dependent diabetes due to autoimmune destruction of pancreatic β -cells and subsequent lack of insulin secretion. In contrast, T2DM is generally referred to as insulin-independent and is characterized by insulin resistance and relative insulin deficiency (Rossi, 2004). The prevalence of T2DM far exceeds that of T1DM, accounting for approximately 90% of diabetes cases and has been closely linked to westernized diets and sedentary lifestyles (Ma and Tong, 2010). Furthermore, the prevalence of diabetes worldwide has more than doubled from 1980 to 2008 (Danaei et al., 2011) and in the United States has almost quadrupled (www.cdc.gov/diabetes; accessed on 7-Aug-2015). Patients with diabetes have a reduced life expectancy by 10 years and reduced quality of life from related complications (Public health agency of Canada, 2011).

Diabetes is diagnosed in patients presenting with classic symptoms of polydipsia, polyuria, polyphagia and weight loss or evidence of vision loss (retinopathy), renal failure (nephropathy) or peripheral nerve dysfunction (neuropathy) (Rossi, 2004). Determination is confirmed through blood tests with a fasted blood glucose (FBG) > 7.0mmol/L or by a blood glucose >11.1mmol/L, 2 hours after a 75g oral glucose

tolerance test. Patients with a FBG between 5.6-6.9mmol/L are considered to have impaired fasting glucose and indicate a pre-diabetic state, at risk for developing DM. Additionally, glycated hemoglobin (HbA1c) levels may be used for diagnosis, however it is more commonly used to assess how well diabetes is managed. In healthy individuals, normal HbA1c levels range from 4% to 5.6%, while those between 5.7% and 6.4% are considered at risk for developing diabetes. HbA1c levels >6.5% are considered diabetic and are at risk for developing complications associated with diabetes (Vijan, 2011). Experts recommend diabetic patients have their HbA1c tested at least twice a year (WHO, 2011).

Diabetes specialists believe a large portion of patients diagnosed with T2DM have had elevated blood glucose levels up to 10 years before diagnosis (www.diabetesdigest.com; accessed on 7-Oct-2015). This a huge concern as damage to the heart, eyes, kidneys and nerves may have already begun. Current understanding of the pathophysiology of T2DM suggests progression of diabetes proceeds through 4 stages characterized by changing blood glucose and insulin levels (Weir et al. 2004). Under normal, healthy conditions (stage A) both blood glucose and insulin levels are found in low concentrations. Progression to Stage B (compensation) is characterized by increased insulin secretion necessary to maintain normoglycemia in response to insulin resistance. Persistent insulin resistance then leads to stage C (decompensation) in which hyperinsulinemia is no longer able to maintain normoglycemia. Prolonged pancreatic stress ultimately leads to a loss of β -cell mass and subsequent decreased insulin secretion that is characteristic of stage D (severe decompensation). Movement between stages may occur in both directions in response to dietary and lifestyle changes.

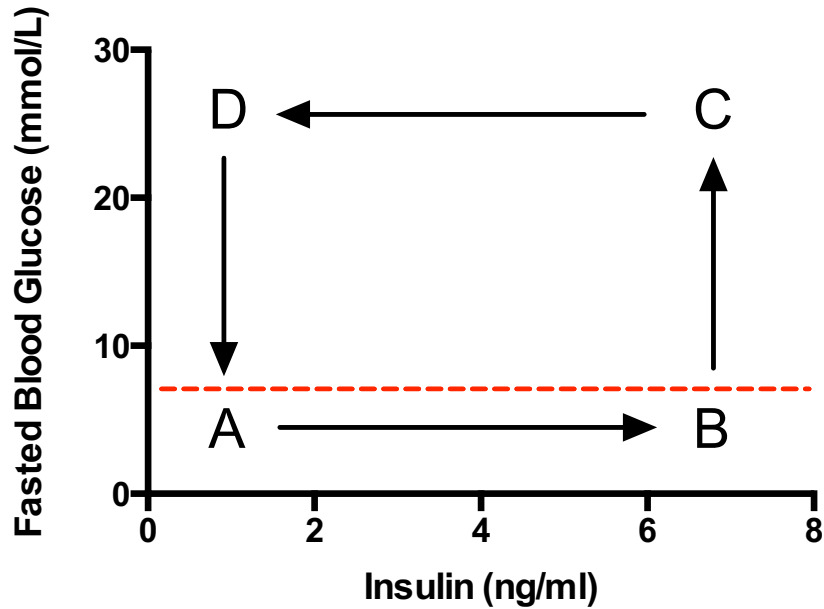


Figure 1.1: Schema representing the progression of T2DM.

Stage A represents healthy individuals with low FBG and insulin levels. Stage B (compensation) represents increased insulin secretion sufficient to maintain normoglycemia. Stage C (decompensation) represents insulin resistant individuals no longer able to maintain normoglycemia. Stage D (severe decompensation) represents reduced β -cell mass and subsequent insulin secretion seen in the late stages of T2DM. The red dotted line represents the hyperglycemic cutoff for humans, 7.0mmol/L.

Long-term complications of DM are separated into two categories: macrovascular and microvascular complications. Macrovascular complications, such as coronary artery disease, peripheral arterial disease and stroke are closely related to elevated mortality rates in diabetics, whereas microvascular complications, such as retinopathy, nephropathy and neuropathy are more closely related to reduced quality of living (Fowler, 2008). Despite significant advances in diabetes care and prevention, diabetes

remains the leading cause of blindness, amputation and kidney failure (ADA diabetes statistics, 2007).

1.2) Diabetic Retinopathy

Diabetic retinopathy (DR) is the leading cause of blindness in working aged adults (Thylefors et al. 1995). With diabetes now considered a worldwide epidemic, the incidence of DR (the most common microvascular complication) is expected to climb to startling levels across the globe. Risk of developing DR is positively linked to both duration and severity of hyperglycemia (Matthews et al. 2004). For this reason, nearly all T1DM patients and about 60% of T2DM patients will have some degree of DR after 20 years (Robinson et al. 2012). Furthermore, of all the microvascular complications, DR has the strongest correlation with elevated HbA1c levels (Cheng et al. 2009).

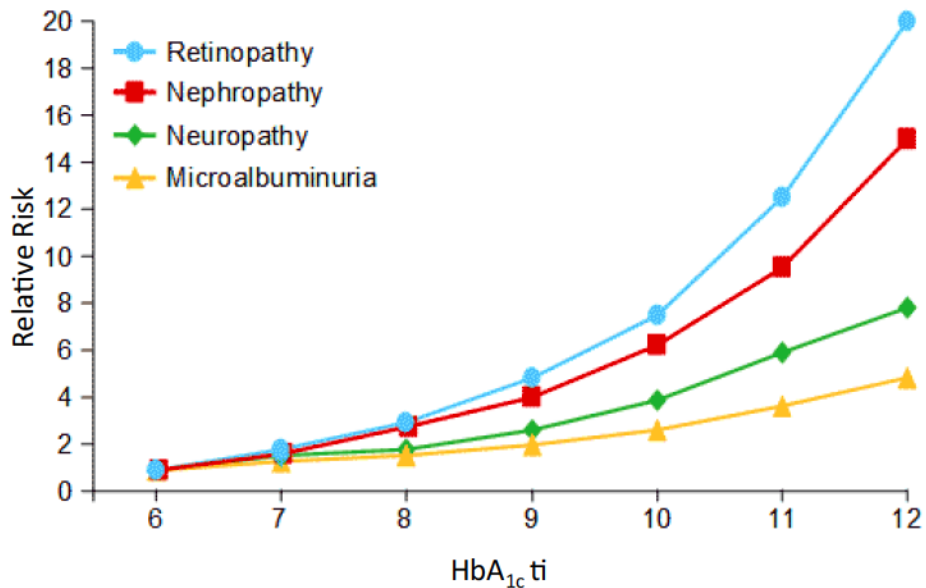


Figure 1.2: Relative risk of developing microvascular complications.

From *DCCT. Diabetes 1995;44:968-43.*

Clinically, DR is categorized as either non-proliferative diabetic retinopathy (NPDR) or proliferative diabetic retinopathy (PDR). NPDR is the earliest stage of the disease and can be further subdivided into 3 degrees of severity. Mild NPDR is indicated by the presence of at least 1 microaneurysm. Moderate NPDR includes more than 1 microaneurysm, occluded vessels and retinal hemorrhages. Severe NPDR is defined as retinal hemorrhages and microaneurysms in all 4 quadrants, occluded vessels, venous beading, cotton wool spots and hard exudates. PDR is the latest and most severe stage of DR, which is characterized by the formation of new blood vessels (neovascularization). Immature blood vessels are highly tortuous and fenestrated, leading to excessive leakage in the eye. This can lead to swelling and causing blurring of vision or blindness in the most severe cases (NEI; accessed on 7-Aug-2015).

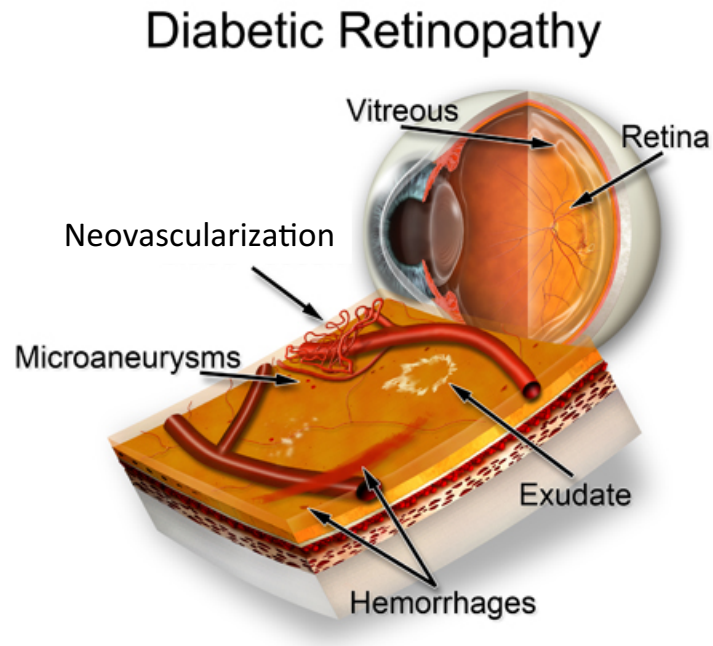


Figure 1.3: Diabetic retinopathy clinically detectable features.

Stages of DR are determined by the frequency and severity of morphological features. Adapted from *Dambrosio eye care Inc.*

Treatment of DR is limited primarily to PDR, while better glucose control has been shown to delay further progression of the disease at all stages (DCCT, 1993). According to the UKPDS, in T2DM patients “each 1% absolute reduction in mean A1C levels was associated with a 37% decrease in the risk of microvascular complications” (Stratton et al. 2000). Common treatments for PDR include laser panretinal photocoagulation to seal or destroy leaky vessels and intra-vitreous injections of anti-vascular endothelial growth factor (anti-VEGF), such as Ranibizumab (Lucentis; Genentech/Roche, South San Francisco) to prevent reformation of immature blood vessels. Treatment of the earlier stages of DR is not needed unless the macula becomes affected (NEI; accessed on 9-Aug-2015)

Furthermore, diabetic patients are at a greater risk of developing eye related disorders such as cataracts and glaucoma (Klein et al. 1995a and Jeganathan et al. 2008). Cataracts appear as a clouding of the lens, resulting from crosslinking of crystalline proteins within the lens. These linkages will absorb light, limiting the amount that will reach the retina, reducing visual acuity. While cataract formation is a natural part of aging, those with diabetes often develop cataracts earlier and more severely than non-diabetics (Klein et al. 1995b). Glaucoma is a condition characterized by increased intra-ocular pressure and subsequent optic nerve (transmit visual signals to the brain) damage. If left untreated, glaucoma can result in permanent blindness. People with diabetes are

twice as likely to develop glaucoma compared to non-diabetics (NEI; accessed on 9-Aug-2015).

1.3) Retinal Microvasculature

Microvasculature consists of pre-capillary arterioles, capillaries and post-capillary venules (Allt, 2001 and Sims, 1986). Associated with these blood vessels are two distinct cell types: (i) endothelial cells (EC) that form the lumen of the capillaries and (ii) pericytes, which provide support for the microvasculature. ECs are adjoined to one another through tight junctions. Pericytes, which are located extra-luminally, contain processes that reinforce EC tight junctions by wrapping around them. The cell bodies of pericytes to ECs are held in close proximity through cell-to-cell junction proteins. These include N-cadherin's, integrin's, adhesion plaques and connexin 43 for the transmission of nutrients, metabolites, secondary messengers and ions between the two cell bodies (Gerhardt et al. 2000 and Bobbie et al. 2010). Additionally, several signaling cascades are necessary for initiating and maintaining functional crosstalk between pericytes and ECs (Winkler et al. 2011). These include: a) Notch, which is primarily involved in embryonic vascular development (Hofmann and Iruela-Arispe et al. 2007); b) platelet-derived growth factor B (PDGF-B), which is essential for the recruitment of pericytes (Lindahl et al. 1997); C) transforming growth factor- β (TGF- β), which is involved in pericyte adhesion and differentiation (Walshe et al. 2009); c); and d) angiopoietin-1 (Ang1), which assists in EC stabilization through activation of the tyrosine kinase receptor, Tie2 (Saharinen et al. 2008). In contrast, angiopoietin-2 (Ang2) promotes pericyte separation

by inhibiting Tie2 (Hammes et al. 2004). As a result, the isolated EC is able to proliferate if exposed to the appropriate angiogenic factors, leading to neovascularization.

Pericyte coverage of the endothelium is specific to each capillary network of the body (Tilton et al. 1979). These differences are the result of varying pericyte-to-endothelial cell (P:EC) frequencies. For example, vascular beds of skeletal muscle have a 1:100 ratio compared to 1:3 and 1:1 ratio found in the brain and retina, respectively (Shepro et al. 1993). The CNS (retina specifically) is believed to have the greatest pericyte coverage due to their involvement in maintaining the blood-brain barrier and blood-retinal barrier. Anatomical differences in pericyte coverage specify the functional attributes of the vasculature (Armulik et al. 2005). In the choroid of the eye, pericyte coverage is minimal, allowing maximal gas and metabolite exchange with surrounding tissue. In contrast, the inner retinal vasculature contains the highest concentration of pericytes to carefully regulate what enters the inner eye.

Originally, pericytes were believed to be exclusively involved in regulation of EC tight junctions (Hellström et al. 2001). Recent evidence suggests pericyte function is much more diverse and dynamic. In the CNS, pericytes are able to facilitate extra-cellular matrix breakdown by expressing metalloproteinases (MMP), removing a physical barrier and promoting angiogenesis (Candelario-Jalil et al. 2009). Interestingly, they are also able to secrete tissue inhibitor of metalloproteinase 3 (a potent inhibitor of several MMPs) and laminin, nidogen and fibronectin, promoting extra-cellular matrix reformation and vascular stability (Saharinen et al. 2008). Pericytes are

also able to regulate capillary blood flow through secretion of vasoconstrictors, such as catecholamines, endothelin-1, vasopressin and angiotensin II as well as through active contraction of actin filaments found within pericyte processes (Hamilton et al. 2010 and Winkler et al. 2011).

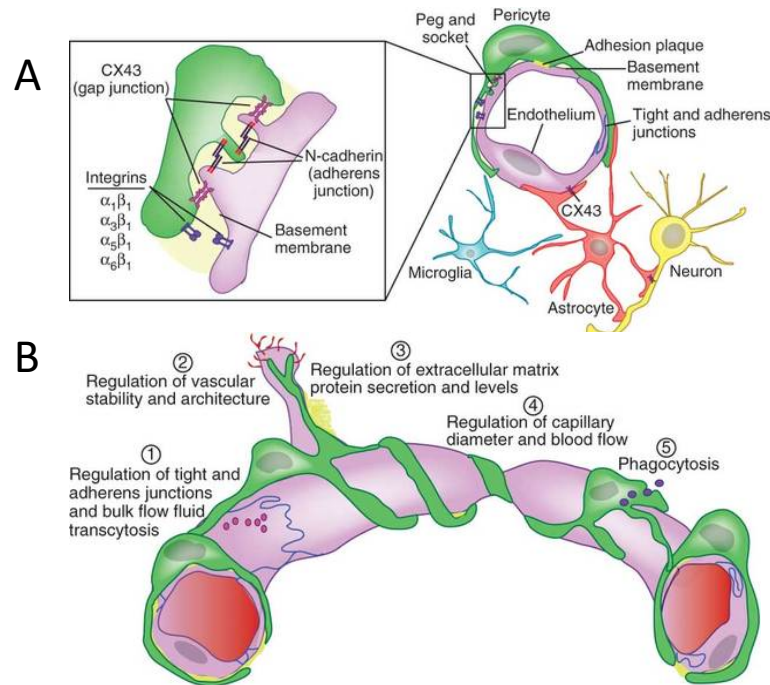


Figure 1.4: Pericyte/endothelial cell structural and functional roles.

A) Illustration of the key junction proteins found between inner retinal pericyte and endothelial cells and B) diverse functional roles of pericytes. From *Winkler et al. (2011)*.

1.4) Cellular Mechanism of Diabetic Retinopathy

Current understanding of the exact cellular mechanism underlying DR still remains incomplete. Traditionally DR was viewed as a disease affecting small blood vessels (microangiopathy), however recent evidence suggests both neuronal cells and

blood vessels are affected, leading to a more accurate definition of a neurovascular disease (Qian et al. 2011). DR is characterized by two hallmark findings: microvascular leakage and microvascular occlusions

In the earliest stages of NPDR microvascular leakage is preceded by a loss of inner retinal pericytes, evident in trypsin digestion preparations (Frank et al. 2004). This leads to a physical weakening of both capillary walls and EC tight junctions. Capillaries void of pericytes are vulnerable to microaneurysm formation and potential rupturing (Hammes et al. 2002). Furthermore, weakening of EC tight junctions compromises the inner blood-retinal barrier, allowing blood constituents to leak into the eye. This is the most common cause of diabetic macular edema and subsequent blindness in diabetic patients (Klein et al. 1995). The mechanism of hyperglycemia-induced pericyte loss is highly debated, however recent evidence suggests co-elevation of glucose and Ang2 stimulates p53 apoptotic pathways in pericytes (Park et al. 2014).

Microvascular occlusions (MO) lead to capillary non-perfusion and regions of hypoxia, which is closely linked to progression into PDR (Josifova et al. 2010). In response to hypoxia, surrounding tissue will secrete angiogenic factors, such as VEGF, in order to stimulate EC proliferation and neovascularization. Hyperglycemia contributes to MO formation by increasing blood viscosity, stickiness of platelets and especially increasing leukocyte adhesion. Leukocyte adhesion is dependent upon endothelial intracellular adhesion molecule-1 (ICAM-1) for firm adhesion, which is found elevated in STZ-induced diabetes models (Miyamoto et al. 1999). However, diabetic patients have reported both elevated and unaltered levels of ICAM-1 (McLeod et al. 1995 and Hughes et al. 2004), suggesting other factors may play a more important role in MO formation.

Furthermore, elevated ICAM-1 expression in STZ models report more leukocyte adhesion in post-capillary venules, rather than pre-capillary arterials. Adherence beyond the capillary bed could not fully explain the manifestation of capillary non-perfusion (Nguyen and Wong 2009).

Lastly, a number of interconnected pathways have been implicated in the early stages of rodent models of DR. These include, but are not limited to increased polyol pathway activity (Robison Jr. et al. 1989), PKC activation (Aiello et al. 1997), advanced glycation end-product (AGE) production (Hammes et al. 1998), inflammation (Miyamoto et al. 1998) and oxidative stress (Kuroki et al. 1996). However, these theories still require further conclusive evidence of their role in the pathogenesis of human DR (Frank, 2004).

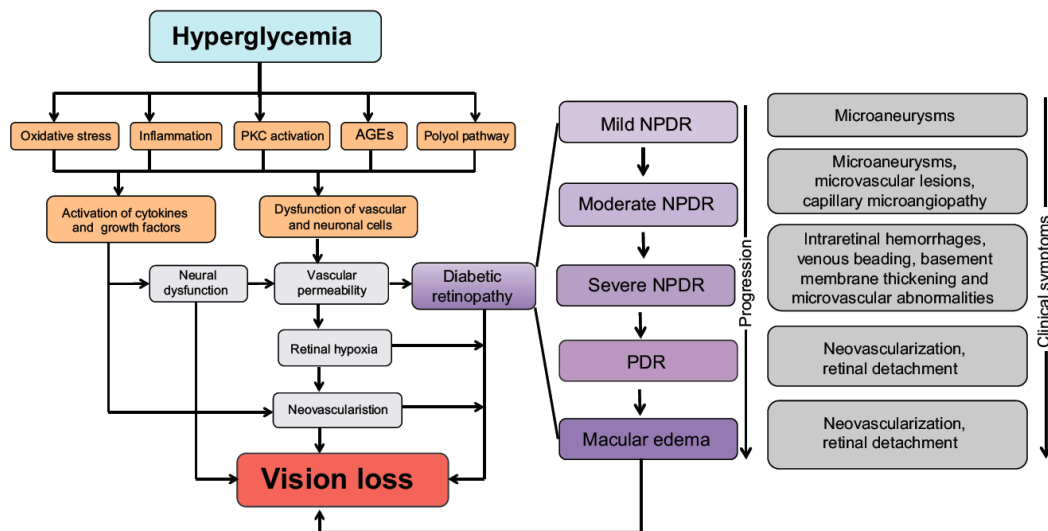


Figure 1.5: Flow diagram of the proposed key factors involved in the pathogenesis of diabetic retinopathy and associated clinical signs.

Adapted from *Robinson et al. (2012)*.

1.5) Current Animal Models of Diabetic Retinopathy

Animal models of DR range from zebrafish to mice and rats and rabbits to dogs and cats to non-human primates. Mice and rats are more commonly used due to their

relative ease of use, short life span and extensive genomic knowledge (Lai and Lo 2013). While they do contain similar features with the early stages of human DR; they do not exhibit all the features of later stages. For instance, early-stage pericyte loss is found in mice and rat models, however late-stage features, such as hard exudates and neovascularization, have not been observed outside of non-human primates (Kim et al. 2004).

The most widely used method of inducing diabetes is through injections of streptozotocin (STZ), which is toxic to pancreatic beta cells and results in cell death. Varying phenotypes may be established through different doses of STZ and/or administration of exogenous insulin to delay the onset of hyperglycemia. The standard protocol for C57Bl/6 mice recommends an intra-peritoneal (IP) injection of 50mg/kg for 5 sequential days (www.diacomp.org: accessed on 5-Aug-2015). An advantage of this method is the quick induction of hyperglycemia, which can be seen as early as 1 week after injection (Lai and Lo, 2013). Furthermore, the classic histopathological features of human DR (pericyte loss and degenerated capillaries) are seen shortly after induction. However, there are limitations to this method. As a model of T1DM, it represents only 10% of total diabetic cases. Additionally, concerns have been raised about the direct toxic effect of STZ on ECs (Taylor et al. 1994). Lastly, retinal thinning seen in these rodent models (Martin et al. 2004), opposes the retinal thickening (edema) seen in post-mortem analysis of diabetic eyes (Reznicek et al.2011).

Alternatively, spontaneous hyperglycemia may be produced through genetic manipulation. The Ins^{Akita} mouse is a T1DM model resulting from a single point mutation (Tyr7Cys) in the insulin 2 gene (Lai and Lo, 2013). As a result of this mutation the disulfide bond bridging between the A and B chains of insulin are lost, inducing severe conformational changes and reduced insulin secretion (Wang et al. 1999). However, despite containing important features of DR, such as degenerated capillaries and increased vascular permeability, the Ins^{Akita} mouse does not exhibit pericyte loss and does exhibit retinal thinning, as seen in STZ models (Kern et al. 2008).

Spontaneous mutations in mice can also lead to models resembling T2DM, as is the case with the db/db mouse. These mice spontaneously develop hyperglycemia due to a deficiency in leptin receptor activity. As a result, these mice excessively eat, becoming obese and hyperglycemic around 1-2 months of age (Hummel et al. 1966). Associated vascular abnormalities are typically seen after approximately 4-5 months of hyperglycemia. These abnormalities include pericyte loss, degenerated capillaries, basement membrane thickening and BRB dysfunction (Cheung et al. 2005). However, these mice are rarely used in DR studies due to difficulty in breeding. Both male and female mice are reported to have insufficient mating performance (<http://jaxmice.jax.org/>; accessed on 7-Aug-2015).

As technology furthers, our ability to create and utilize various models increase. These models are very important for our understanding of disease pathogenesis in humans, as well as for screening novel therapeutic treatments (Lai and Lo, 2013). Yet, these models are limited by their differences from humans. Models that more accurately

resemble all aspects of human DR are essential for a complete understanding of the mechanism involved in DR.

1.6) Nile Grass Rat Background

The Nile grass rat (NR), *Arvicanthis niloticus*, is a herbivorous murine rodent, which naturally inhabits the dry savannah, tropical and subtropical grasslands of Africa (Blanchong et al. 1999). They feed primarily upon vegetative plants, grass seeds and small insects. Unlike most rodents, which are nocturnal, the NR is primarily crepuscular (Delany and Kansimeruhanga 1970). Additionally, NR photoreceptors are ~35% cones, compared to the 1-3% found in mice and rats (Bobu et al 2006). Classically, the NR was used as a model for studying circadian rhythm (Blanchong et al. 1999), however recently Noda et al. 2010 and Chaabo et al. 2010 introduced this rodent as a model for Mets/T2DM. These reports both suggest the NR contains many of the systemic pathological complications associated with human T2DM, such as hyperinsulinemia, elevated plasma triglycerides and cholesterol, hypertension, liver steatosis, nephropathy and atrophy of pancreatic islets. Furthermore, Noda et al. 2014 introduced retinopathy in the NR and provided novel findings to the understanding of inflammation in DR. Compared with commonly used STZ-models, hyperglycemic NRs revealed less leukocyte adhesion in advanced diabetes and also found leukocyte adhesion primarily in arterioles, rather than venules (seen in STZ models). Hyperglycemic NRs exhibited the classic signs of endothelial cell damage, obliterated capillaries and pericyte ghosts. Taken together these findings suggest the NR will make a suitable model to further our understanding of the pathogenesis of DR.

1.7) Fundus Imaging

Diabetic retinopathy does not reduce vision until the latest stages of the disease. Unfortunately, by this point treatment is limited and may only help delay inevitable vision loss. Thus, delaying and perhaps preventing blindness, requires detection of an asymptomatic disease by imaging the retina (Viswanath and McGavin 2003). This is achieved through fundus examination and is encouraged for all diabetic patients routinely. A specialized low power microscope with an attached camera (fundus camera) allows visualization of retina and associated inner retinal vasculature. Microaneurysms, hemorrhages, hard exudates, venous beading and neovascularization are all detectable using this technique and is used for the standard grading system of DR, previously described. Fundus imaging may be combined with a small intravenous injection of fluorescein (intravenous fluorescein angiogram) in order to enhance visualization of inner and choroidal vasculature and associated complications such as occlusions and leakage.

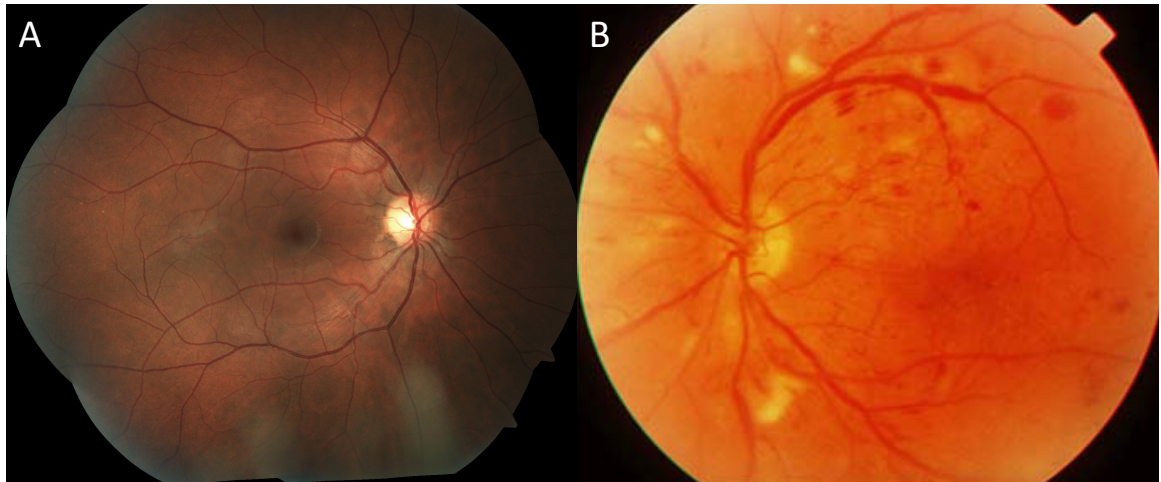


Figure 1.6: Fundus imaging of a healthy and diabetic retina.

Representative images of a healthy (A) and diabetic (B) retina characterized by severe NPDR.

1.8) Electroretinogram

The Electroretinogram (ERG) records summated electrical responses of the retina to brief flashes of light. Recording electrodes placed at the level of the cornea measure membrane potential changes in relation to subdermally located ground electrodes behind each eye. Acquired responses produce a waveform consisting of: a negative deflecting a-wave, followed by a positive deflecting b-wave. The a-wave corresponds to the hyperpolarization of photoreceptors in response to light, while the b-wave represents the depolarization of ON-bipolar cells. A-wave amplitudes are measured from the baseline to the trough of its negative peak, while b-wave amplitudes are measured from the trough of the a-wave to the following maximal peak. Implicit time of each wave is defined as the time from flash onset to their respective peak. Furthermore, superimposed over the ascending limb of the b-wave is 4 to 6 low-amplitude, high-frequency wavelets called oscillatory potentials (OP). These oscillations are believed to represent feedback between

amacrine cells and bipolar or ganglion cells. Frequently, individual wavelets are analyzed from peak to trough for both amplitude and implicit time. These individual wavelets are referred to as OP1-4 with respect to the first, second, third and fourth peak.

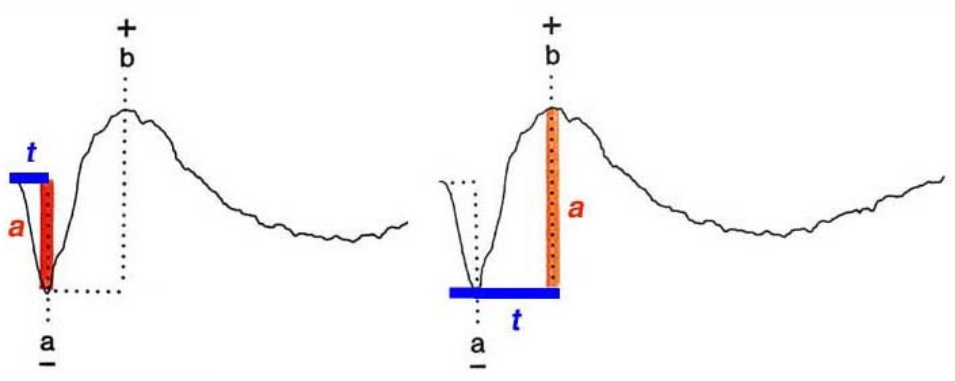


Figure 1.7: Amplitude and implicit time measurements of the ERG waveform.

A-wave amplitudes are measured from the baseline to the trough of its negative peak, while b-wave amplitudes are measured from the trough of the a-wave to the following maximal peak. Implicit time of each wave is defined as the time from flash onset to their respective peak. Adapted from *webvision.med.utah.edu*

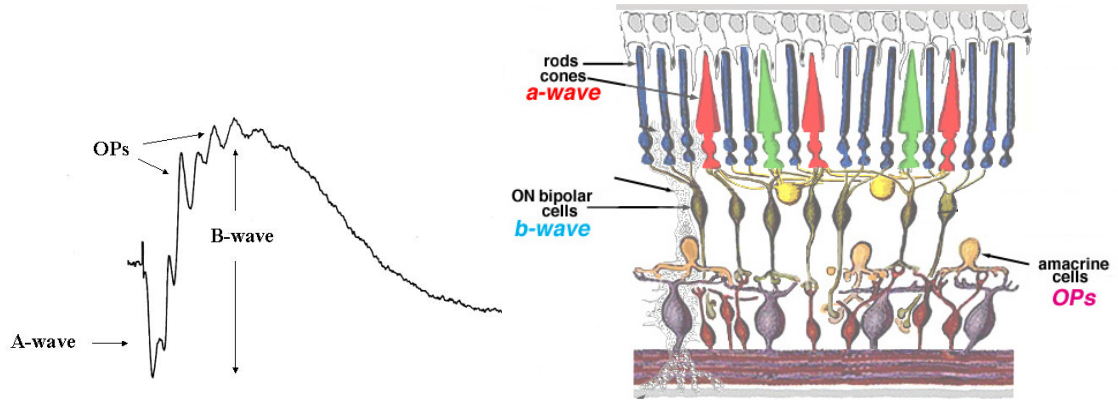


Figure 1.8: Components and origin of the ERG waveforms.

The negative a-wave corresponds to photoreceptor hyperpolarization. The positive b-wave corresponds to depolarization of ON bipolar cells. High frequency oscillations superimposed on the b-wave correspond to amacrine cell activity. Adapted from *webvision.med.utah.edu*

Multiple ERG protocols have been established through altering the brightness and frequency of light stimulation. By controlling variables such as the background illumination, flash intensity, wavelength and duration, it is possible to isolate rod and cone responses, ON- (shortly after light onset) and OFF- (shortly after light offset) responses and also pre- and post-synaptic responses. Thus, the ERG is an invaluable tool for detecting distinct functional changes of the retinal circuitry.

1.9) The Electroretinogram in Diabetic Retinopathy

The ERG is a non-invasive objective method for evaluating the functional status of the diabetic retina (Tzekov and Arden, 1999). Three distinct ERG abnormalities have been identified in patients with DM at different stages of the disease. The first and

earliest detectable change that is commonly seen before any visible changes in the fundus is an increased OP1 implicit time. Additionally, reduced OP amplitudes are seen in the early and also later stages of DR (Movasat et al. 2008). Secondly, late-stage DR patients take longer to dark-adapt and have higher scotopic threshold responses (Arden et al. 1999 and Henson et al. 1979). Lastly, DR patients have exhibited significantly lower mesopic contrast sensitivity responses, while maintaining good visual acuity (Katz et al 2010).

Chapter. 2 RESEARCH PLAN

2.1) Rationale

Diabetic retinopathy is the leading cause of blindness in working-aged adults. Legally, blindness is defined as those with a central visual acuity of 20/200 or less (AFB 2008). High visual acuity is achieved through dense concentration of cone photoreceptors in the fovea of the retina. Despite the human retina containing only 5% cones, all photoreceptors found within the fovea are cones and allow for color perception, daylight and fine detailed vision. Disruption and/or death of these photoreceptors and related circuitry will result in diminished visual acuity and potentially blindness (as seen in DR). The primary concern of eye care is to preserve this crucial component of vision (NEI; accessed on 9-Aug-2015). Studies concerned with cone preservation would be ideally commenced in cone-based diurnal animals, such as guinea pigs (8-17% cones; Peichl and Gonzalez-Soriano, 1994), ground squirrels (70-90% cones; Kryger et al. 1998) or tree shrews (86-99% cones; Müller and Peichl, 1989). However, the most commonly used models (mice and rats) are nocturnal animals that contain only 1-3% cones, but are used due to their relative ease of use, fully known genomic sequence, ease of genetic manipulation, decades of deep knowledge regarding their physiology and short life span (Lai and Lo, 2013).

The NR offers several advantages over the less than ideal mice and rat models. As crepuscular animals their retinas contain approximately 35% cones (Gaillard et al. 2009). Furthermore, recent reports have shown elevated spatial acuity, as measured by optokinetic (heading turning) behavior (Gaillard et al. 2008). Lastly, ERG recordings in NRs have reported five-fold larger photopic a-wave amplitudes, which more closely

resembles human foveal vision (Gilmour et al. 2008). Taken together these findings suggest the NR would be a superior model for studying cone-based foveal vision.

The most widely used animal model of DR is the STZ rat/mouse. STZ induces pancreatic β -cell death (similar to T1DM) and rapid onset of hyperglycemia and related retinopathy shortly after. However, these models do not resemble the slow time course of DR development in humans. Slow progressing T2DM models characterized by insulin resistance and relative insulin deficiency are limited. Currently, the sand rat is the only reported model of spontaneous T2DM that exhibits features of DR (Saïdi et al. 2011). However, the inability to maintain a colony has hindered investigation of this animal model. NRs on the other hand, do breed in captivity and are currently used in circadian rhythm studies (Katona et al. 1997 and Shuboni et al. 2012). Additionally, Noda et al. 2010 and Chaabo et al. 2010 demonstrate the susceptibility of the NR to develop a slow naturally progressing “Metabolic Syndrome that evolve into diet-induced non-insulin-dependent (type 2) diabetes mellitus”. Furthermore, they reveal a number of systemic complications (liver steatosis, abdominal fat accumulation, nephropathy, atrophy of pancreatic islets, hypertension and elevated plasma triglycerides and cholesterol) found in the NR that are commonly seen in human T2DM patients. The NR provides a unique “...opportunity of combining the cone-rich aspect and the potential of modeling human diabetic retinopathy” (Dr. Stell).

2.2) Hypothesis

I propose that Nile grass rats fed standard lab chow will develop hyperglycemia and associated retinal vasculopathy resembling features of human diabetic retinopathy.

This hypothesis predicts the following morphological retinal changes in hyperglycemic retinas:

- 1) A reduced number of vascular pericytes
- 2) An increased number of degenerated capillaries
- 3) Formation of microaneurysms
- 4) Microvascular leakage

2.3) Objectives

A main goal of this study is to assess the NRs potential as a new model for studying human DR. To satisfy this goal the vascular abnormalities present only in hyperglycemic and not normoglycemic NR retinas, will be compared to the classic histopathological signs of human diabetic retinopathy. The premise of using the NRs over current animal models, such as STZ mice or rats, is the slow time course of HG (resembling human T2DM), which will allow us to decipher the mechanisms involved in HG-induced complications. Furthermore, the cone-based crepuscular vision of the NR provides a unique opportunity to further our understanding cone-based vision that is so essential to human vision.

Chapter. 3 EXPERIMENTAL DESIGN AND METHODS

3.1) Experimental Design

3.1A) Animals

The experimental study was performed on male and female Nile rats aged 6 to 18 months of age. All outcome measures were compared between normoglycemic (Mazuri fed) and hyperglycemic (Prolab 2000 fed) Nile rats raised in the animal facility of the University of Alberta, under a 12 : 12 light-dark cycle and housed in polycarbonate cages filled with aspen chips, large aspen shavings, krinkle paper and a PVC tube. Pups were weaned at 3 weeks of age, at which point they were given one of two diets and separated based on sex into new cages (1-4 animals/cage). Food and water were provided *ad libitum* in an environment with humidity and temperature of 50% and 22°C, respectively. Experiments were carried out in accordance with the Institutional Animal Care and Use Committee (University of Alberta; license no. 463) and the ARVO (Association for Research in Vision and Ophthalmology) Statement for the Use of Animals in Ophthalmic and Visual Research.

3.2B) Dietary Manipulation

Glycemic status was manipulated through dietary means. The first group of Nile rats was fed standard rodent laboratory chow (Prolab RMH 2000 – 5P06) containing 9.6% fat, 3.2% fiber, 19.9% protein and 50.8% carbohydrates. A second group of Nile rats was fed a high fiber, low energy diet (Mazuri Chinchilla – 5M01) containing 4.1% fat, 15% fiber, 21% protein and 42.5% carbohydrates. Both groups were fed their

designated diet from birth. Based on preliminary results Nile rats fed Mazuri Chinchilla were expected to maintain normoglycemia and would serve as controls, where as those fed Prolab 2000 were expected to develop hyperglycemia. Both diets were nutritionally complete. Glycemic status was determined through fasted blood glucose and glycated hemoglobin (HbA1c) levels.

Table 1: Nutritional composition of the Mazuri chinchilla and Prolab 2000 diet

Mazuri® Chinchilla Diet

Nutrients		Minerals	
Protein, %.....	20	Ash, %.....	6.9
Arginine, %.....	1.2	Calcium, %.....	0.90
Cystine, %.....	0.28	Phosphorus, %.....	0.67
Histidine, %.....	0.49	Potassium, %.....	1.7
Isoleucine, %.....	1.1	Magnesium, %.....	0.3
Leucine, %.....	1.5	Sodium, %.....	0.26
Lysine, %.....	1.1	Chloride, %.....	0.55
Methionine, %.....	0.53	Iron, ppm	350
Phenylalanine, %.....	1.0	Zinc, ppm	119
Tyrosine, %.....	0.67	Manganese, ppm	95
Threonine, %.....	0.80	Copper, ppm	15
Tryptophan, %.....	0.28	Iodine, ppm	0.87
Valine, %.....	1.0	Selenium, ppm	0.30
		Cobalt, ppm	1.2
Fat (Ether extract), %.....	4.1		
Linoleic Acid, %.....	1.6		
		Vitamins	
Fiber (Crude), %.....	15	Thiamin, ppm	4.9
Neutral Detergent Fiber, %.....	29	Riboflavin, ppm	5.6
Acid Detergent Fiber, %.....	17	Niacin, ppm	48
Starch, %.....	9.8	Pantothenic acid, ppm	19
Glucose, %.....	0.21	Choline, ppm	1,710
Fructose, %.....	0.75	Folic acid, ppm	9.8
Sucrose, %.....	2.61	Pyridoxine, ppm	7.6
Lactose, %.....	0.56	Biotin, ppm	0.25
		Vitamin B ₁₂ , µg/kg	12
Metabolizable Energy,		Vitamin A, IU/kg	33,440
kcal/kg	2,910	Vitamin D ₃ , IU/kg	1,780
		Vitamin E, IU/kg	230
		Vitamin K, ppm	2.7
		Beta-carotene, ppm	15

Prolab® RMH 2000

Nutrients		Minerals	
Protein, %.....	19.9	Ash, %.....	6.5
Arginine, %.....	1.10	Calcium, %.....	0.80
Cystine, %.....	0.27	Phosphorus, %.....	0.81
Glycine, %.....	1.12	Potassium, %.....	1.08
Histidine, %.....	0.43	Magnesium, %.....	0.23
Isoleucine, %.....	0.92	Sodium, %.....	0.48
Leucine, %.....	1.45	Chloride, %.....	0.75
Lysine, %.....	1.03	Iron, ppm	440
Methionine, %.....	0.33	Zinc, ppm	150
Phenylalanine, %.....	0.82	Manganese, ppm	120
Tyrosine, %.....	0.52	Copper, ppm	15
Threonine, %.....	0.72	Iodine, ppm	1.4
Tryptophan, %.....	0.25	Selenium, ppm	0.14
Valine, %.....	0.98	Cobalt, ppm	0.37
Serine, %.....	0.98		
Aspartic Acid, %.....	1.78		
Glutamic Acid, %.....	4.68	Vitamins	
Alanine, %.....	0.93	Thiamin, ppm	7.9
Proline, %.....	1.66	Riboflavin, ppm	12
Taurine, %.....	0.01	Niacin, ppm	54
		Pantothenic acid, ppm	16
Fat (Ether extract), %.....	9.6	Choline, ppm	1,800
Cholesterol, ppm	78	Folic acid, ppm	0.90
Linoleic Acid, %.....	4.93	Pyridoxine, ppm	5.4
Linolenic Acid, %.....	0.70	Biotin, ppm	0.29
Omega-3 Fatty Acids, %.....	0.76	Vitamin B ₁₂ , µg/kg	15
		Vitamin A, IU/kg	19,000
Fiber (Crude), %.....	3.2	Vitamin D ₃ , IU/kg	1,500
Neutral Detergent Fiber, %.....	12.3	Vitamin E, IU/kg	49
Acid Detergent Fiber, %.....	4.4	Vitamin K, ppm	1.3
Starch, %.....	25.7	Beta-carotene, ppm	2.0
Glucose, %.....	0.0		
Fructose, %.....	0.1		
Sucrose, %.....	0.6		
Lactose, %.....	9.0		
		Metabolizable Energy,	
		kcal/kg	3,520

Adapted from http://www.mazuri.com/products_pdfs/5M01.pdf

www.labdiet.com/cs/groups/lolweb/@labdiet/documents/web_content/mdrf/mdi4/~edisp/ducm04_028421.pdf

3.2 Tissue Collection

3.2A) Blood Collection

At each of the three experimental terminal endpoints (6mo, 12mo or 18mo), Nile rats were euthanized with an intra-peritoneal (IP) injection of 0.2 mL of Euthanyl (Bimeda-MTC Animal Health Inc., Cambridge, ON, Canada). After assurance that the animals had reached surgical plane (by the lack of toe-pinch response) the chest cavity

was opened up, exposing the heart. Using a 23-gauge needle to puncture the apex of the heart's left ventricle, 1mL of blood was collected. Whole blood was immediately transferred to potassium (K) and sodium (Na) ethylenediaminetetraacetic acid (EDTA) tubes in equal quantities and centrifuged at 2000rpm for 20 minutes at 4° C. Aprotinin (A6279, Sigma-Aldrich Co., St. Louis, MO, USA) was added to both KEDTA and NaEDTA tubes at 55µL/mL of blood to prevent degradation of peptide hormones. Plasma and packed blood cells from both KEDTA and NaEDTA tubes were separated and immediately flash frozen in liquid nitrogen in 200µL aliquots and stored at -80°C.

3.2B) Ocular Tissue Collection

Following blood collection *via* cardiac puncture both eyes were enucleated (by sliding a pair of surgical scissors inside the orbits) and immediately immersed in 4% paraformaldehyde (PFA) for 30 minutes. After this period, the cornea was punctured with a scalpel (surgical blade stainless, No.11, Feather Safety Razor Co. LTD, Osaka, Japan) and the cornea and lens were removed. The remaining eyecup (excluding retinal flat mounts) was then re-immersed in 4% PFA for an additional 30 minutes, followed by treatment with a sucrose gradient. Beginning with 10% sucrose, followed by 20% sucrose for one hour and concluding with 30% sucrose overnight at 4°C. Prior to embedding the tissue, the eyecup was rinsed in O.C.T freezing compound (Sakura Finetek USA Inc., cat. #4583, Torrance, CA, USA) to remove excess sucrose and then placed into a plastic cryomold filled with O.C.T freezing compound. Eyes were carefully oriented in the cryomold, with the anterior aspect facing forward. The cryomold was placed on top of an

aluminum channel stand immersed in liquid nitrogen, allowing progressive freezing of the eye and then sub sequentially stored at -80°C.

3.2C) Supplementary Tissue Collection

Supplementary tissue was collected for use by other labs, allowing optimal use of each animal. I was in charge of the intricate logistics of coordinating tissue collections by multiple collaborators with respective expertise in diabetes complications.

Pancreas (Dr. Cathy Chan, diabetic pancreatic pathophysiology expert)

Pancreases were collected from male Nile rats aged 6mo, 12mo and 18months. These pancreases were fixed in 4% PFA before being embedded in paraffin. Samples were then sectioned into 5mm serial sections and stained accordingly. Pancreatic islets were isolated from a subset of 12-month-old male Nile rats in order to perform glucose stimulated insulin secretion tests. Isolation involved perfusion in live animals (having received lethal Euthanyl levels) via the bile duct using a solution containing collagenase. Dr. Carina Yang and members of the Chan lab performed all pancreatic analysis.

Lens (Dr. Carlo Montemagno, studying nanotechnology-based cataract removal)

Freshly isolated lenses were transferred to cryogenic vials (Corning, cat. #430488) containing a 20% glycerol buffer solution and flash frozen in liquid nitrogen before being stored at -80°C. The aim being to further our understanding of cataractogenesis.

Kidneys (Dr. Alex Gutsol, nephrologist)

Kidneys were removed from 6, 12 and 18-month-old control and HG NRs. Kidneys were fixed in 4% PFA for 24 hours before being subject to a series of sucrose solutions. Samples were shipped in 30% sucrose to Dr. Gutsol at the University of Ottawa. The aim being to further our understanding of the pathological mechanisms triggering and aggravating diabetic nephropathy.

Dorsal root ganglion and footpads (Dr. Christine Webber, neuropathic pain expert)

A subset of 18-month-old normoglycemic and hyperglycemic Nile rats underwent von-frey filament testing, followed by post-mortem mechanical rod stimulation of peripheral sensory pain fibers (A-delta and C-fibers). Lastly, dorsal root ganglions were collected for immunohistochemistry. The aim being to further our understanding of the mechanisms involved in triggering and progression of diabetic peripheral neuropathy.

Heart (Dr. Helene Lemieux, mitochondrial respiration expert)

Left ventricular walls were dissected out in order to isolate fibers, prior to immersion in oxygraph chambers, designed to be injected with specific metabolic substrates of mitochondrial respiration. The aim being to determine whether or not mitochondrial dysfunction is a key player in the initiation and progression of diabetic cardiomyopathy.

Liver (Dr.Consolato Sergi, pediatric hepato-oncologist)

Whole livers were carefully removed before separating apart the right and left lobe. Each lobe was imaged, weighed, measured and sectioned. The first sectioned was immersed in 4% PFA for 24 hours before being imbedded in paraffin by ADI core services. A second section was flash frozen in liquid nitrogen and stored at -80°C. Lastly, a 2mm x 2mm piece was stored in 1% glutaraldehyde for electron microscopy. The aim being to study the pathophysiology of hepatocarcinoma development in diabetic patients.

Mesenteric artery (Dr. Francis Plane; vascular pharmacologist)

Remaining carcasses were given to Dr. Plane for isolation and stimulation of mesenteric arteries through pharmaceutical means. The aim is to further our understanding of how hyperglycemia impacts the pharmacological properties of blood vessels and the relationship to the development of associated vascular complications.

Together, these multidisciplinary approaches are bound to depict a comprehensive picture of diabetic complications in terms of trigger, progression and most importantly, novel preventative therapies.

3.3) Experimental Methods

3.3A) Whole Body Composition

Whole body compositions were assessed in both groups of NRs in order to determine the effect of diet on bodyweight and fat/lean masses. Fat and lean masses were calculated in relation to bodyweight using Nuclear Magnetic Resonance instrumentation (Echo-MRI 4in1-500).

3.3B) Fasted blood glucose

Fasted blood glucose (FBG) levels were measured from Mazuri and ProLab 2000 fed Nile rats in order to determine their glycemic status. Animals were fasted overnight and given only water for 16-18 hours. After this period, the tip of the tail was snipped using non-serrated hardened fine scissors (F.S.T 14090-09), while a second individual held the NR. The tail was then gently massaged to facilitate blood flow to the end of the tail, allowing application of blood to the Accu-Chek compact plus glucose monitoring system (Roche Diabetes Care Inc., Indianapolis, IN). Due to a high incidence of tail morbidity associated with this technique, animals were euthanized shortly after the procedure, preventing longitudinal measurements of FBG levels. Hyperglycemia cutoff was defined as the average FBG of all Mazuri fed animals (independent of sex and age) plus two times the standard deviation.

This protocol was refined, allowing longitudinal assessment of the FBG levels. Another individual held the Nile rat, while the tip of the tail was punctured with a fine scalpel (No. 11 Feather Safety Razor Co. LTD). Again, the tail was gently massaged to facilitate the application of a single drop of blood to the Contour Next® (Bayer) glucose meter. This technique does not induce tail morbidities and can be used longitudinally.

3.3C) Glycated Hemoglobin

Glycated hemoglobin was measured to estimate the average plasma glucose concentration of the past 3 months. A 50 μ L sample of packed blood cells was placed in a 12x75mm disposable borosilicate glass tube (cat. #14-961-26, Fischerbrand) with 400 μ L of hemolysate compound. The solution was vortexed for 30 seconds and allowed to settle

for a minimum of 5 minutes, but not more than 45 minutes. GLYCO-Tek affinity columns were prepared by up-ending each column twice and re-suspended the resin with a Pasteur pipette, being careful to avoid introducing air bubbles. The supernatant was then drained from the affinity column over a 15mL polypropylene tube, allowing re-compaction of the resin. After the resin had settled to a level of 1.1cm above the filter, the remaining supernatant was removed with a transfer pipette. Lastly, 3mL of Developer A solution was added to the column and allowed to drain. After complete elution, the affinity column was moved to a new 15mL polypropylene tube (labeled non-GHb) and 50µL of the prepared hemolysate solution was applied to the top of the resin bed for incubation. After 8 minutes, 0.5mL of Developer A was added, washing any hemolysate adhering to the sides of the column into the resin. An additional 4mL of Developer A was then carefully added. Following complete elution of Developer A, the affinity column was transferred to a new 15mL polypropylene tube (labeled GHb) and 3mL of Developer B was added to the column. The volume of the non-GHb tube was adjusted to 15mL with reagent grade water. After complete elution of Developer B, both the non-GHb and GHb tubes were inverted a total of 3 times. Duplicates of 1mL samples of non-GHb and GHb were transferred to a 24 well plate and their absorption at 415nm was measured using a standard spectrophotometer (BioTek™ Synergy™ Mx Monochromator-Based Multi-Mode Microplate Readers). HbA1c was calculated according to the following equations:

$$1) \% GHb = \left(\frac{Abs. of GHb tube}{Abs. of GHb tube + 5(Abs. of non - GHb tube)} \right) \times 100$$

$$2) HbA1c = 0.6846 (\% GHb + 0.973258)$$

% GHb = percentage of glycosylated hemoglobin's in the sample

Abs. of GHb tube = absorbance of the contents in the GHb tube at a wavelength of 415nm

Abs. of non - GHb tube = absorbance of the contents in the non-GHb tube at a wavelength of 415nm

HbA1c % cutoff was defined as the average of all Mazuri fed animals (independent of sex and age) plus two times the standard deviation.

3.3D) Plasma Insulin

The effect of diet on pancreatic function was evaluated through measurements of fasted plasma insulin levels. Quantification was achieved by running plasma samples through an insulin ELISA assay kit (Crystal Chem Inc. Downers Grove, IL Ultra Sensitive Mouse Insulin ELISA kite #90080). The kit was run according to the provided instructions by our lab technician, Sharee Kuny.

3.3E) Retinal Digests

In vitro vascular integrity was evaluated using trypsin digestion to isolate the retinal vasculature. Retinal digestion is a commonly used method for qualitative and quantitative assessment of the vasculature, allowing accurate evaluation of capillary endothelial cells and pericytes. The technique described below was amended from the technique described in Dietrich, N., & Hammes, H. 2012, for specific use of NR retinas. I

developed a new method for separating the retina and eyecup, as well as determined optimal digestion times for control and HG retinas. Many hours were devoted to improving the quality of the isolated vascular network.

Frozen right eyes were thawed for 30 minutes at room temperature before immersion in 4% PFA for 17 hours. After this period, the retina was carefully separated from the eyecup and submerged in a 3% trypsin buffer solution (pre-heated to 37°C in a 35x10mm tissue culture dish) for 2 hours and 10 minutes (controls) or 2 hours and 5 minutes (hyperglycemic). Following digestion, the vitreous was removed and the remaining digested retina was washed in reagent grade water until no further cell separation was observed (3- 4 washes). Complete vitreous removal is essential for separation of retinal cells from the vasculature. At this point, the digested retina was transferred to a frosted glass slide (Superfrost plus, cat. no. 12-550-15, Fisher Scientific, USA) outlined with a hydrophobic pen (ImmEdge Pen, cat. #H-4000, Vector Laboratories Inc., Burlingame, CA, USA), using a glass aspirator coated in 3% trypsin buffer solution. Reagent grade water was applied gently on top of the retina using a 26^{1/2} gauge needle in order to facilitate separation of the remaining retinal cells. Using a 200µL pipette, separated retinal cells were removed with excess water, while avoiding disturbance of the vasculature. This process was conducted repeatedly under a Leica M60 dissecting microscope, until no further retinal cells remained visibly attached to the vasculature. The vasculature was then allowed to dry before being incubated in a series of periodic acid solution (SLBC9648, Sigma-Aldrich) for 10 minutes, Schiff's reagent (SLBC9265, Sigma-Aldrich) for 15minutes and hematoxylin solution (SLBC9662, Sigma-Aldrich) for 2 minutes. 1 minutes washes of distilled water, luke warm water and

tap water occurred between reagents, respectively. Lastly, a single drop of fluoromount (091M1261, Sigma-Aldrich) was applied and a glass cover slip was laid over the tissue. To provide sufficient time for slides to cure, they were laid flat overnight and sealed with clear nail polish the following day. Images were captured at 40x with oil immersion using a Reichart Polyvar 2 microscope and infinity-capture imaging software.

Pericytes were identified as round, dark and extracapillary protrusions compared to endothelial cells, which were oval shaped and lighter in color (Dietrich, N., & Hammes, H. 2012). Number of pericytes, endothelial cells and degenerated capillaries were counted and normalized to capillary area using ImageJ software. Furthermore, pericytes were divided into three groups based on their location. Pericytes located on straight capillaries, forked capillaries and bridging between capillaries were classified as longitudinal, forked and bridging pericytes, respectively. Six animals per group were assessed at each time point with the average of 5 randomly selected images per animal being analyzed.

3.3F) Fluorescein Angiography

In vivo vascular integrity was assessed through fundus imaging combined with an injection of fluorescent dye. Animals were anaesthetized with a mixture of 5:2 ketamine (Ketalean, Bimeda-MTC Animal Health, Inc., Cambridge, ONT, Canada): xylazine (X1251, Sigma-Aldrich Co., St. Louis, MO, USA) (75 mg/kg: 30 mg/kg, respectively) via intraperitoneal injection with a 26^{1/2} gauge needle (0.45mm x 13 mm, PrecisionGlide Needle, Becton Dickinson & C., Franklin Lakes, NJ, USA). Eyes were dilated by a

corneal application of 1% tropicamide (Mydracyl, Alcon Laboratories, Inc., Fort worth, TX, USA) and 2.5 % phenylephrine (Bosch & Lomb Pharmaceutical, Inc., Tampa, FL, USA); kept hydrated with tear gels (Ophthalmic liquid gel, Novartis Pharmaceuticals Canada). NRs were then given then a second injection containing fluorescein isothiocyanate (1.5 μ L/g). Images were captured using commercial software (StreamPix5 Software; Phoenix Research Laboratories) and Semrock FF01-469/35; Semrock BLP01-488R filters to avoid auto-fluorescence in the eye and camera lens. Images from both eyes were acquired, however the eye presenting with a greater number of primary vessels (extending from the optic disk) was assessed. The number of primary vessels was quantified at a fixed eccentricity of 0.5x the optic disc diameter. Vessels with a diameter less than 10 μ m were undetectable through cataracts and were excluded from analysis.

3.4) Immunohistochemistry

3.4A) Cross-sections

Anatomical retinal changes were assessed through stained cross-sections of the retina. The cryostat (Leica CM1850, Germany) was set at -25°C to achieve the optimal temperature to perform cryosectioning. Frozen left eyes were cut with a C35 microtome blade (Feather Safety Razor Co., LTD., Japan) into 20 μ m sections along the naso-temporal axis and mounted on frosted glass slides (Superfrost plus, cat. no. 12-550-15, Fisher Scientific, USA). A total of 48 sections were acquired per eye and collected onto 16 separate slides labeled A1-H2, for storage at -20°C.

Sections were blocked in 10% (goat or horse) serum and 0.3% Triton X-100 in phosphate buffered saline (PBS) for 2 hours at room temperature. Six series were stained with either rabbit anti-tyrosine hydroxylase (1:500), goat anti-choline acetyl transferase (1:200), rabbit anti-Cx36 (1:1000), mouse anti-Cx43 (1:1000), mouse anti-GFAP (1:1000) or Dylight 594-labeled tomato lectin (1:100) overnight at 4°C. Sections were then washed in PBS before further staining with either goat anti-rabbit Alexa488 (1:1000), donkey anti-goat Alexa594 (1:500), goat anti-mouse Alexa594 (1:1000) or donkey anti-mouse Alexa594 (1:1000) for 2 hours at room temperature. All series' were then washed in PBS, coated with ProLong[®] Gold anti-fade reagent (Cat. #P36931; Molecular Probes Inc., Eugene, OR, USA) containing the nuclear stain 4, 6-diamidino-2-phenylindole (DAPI) and covered with a glass coverslip (Microscope Cover Glass, 22x50, cat.no. 12-545E, Fisher Scientific, USA). To provide sufficient time for slides to cure, they were positioned flat overnight and sealed with clear nail polish the following day.

Images were captured on a Leica DFC360 FX microscope using a 20x objective lens. Six animals per group were assessed at the center (adjacent to the optic nerve), periphery (adjacent to the ora serrata), and the middle (a location equidistant from the center and periphery) of the retina. The average of 3 measurements per image was used for statistical analysis.

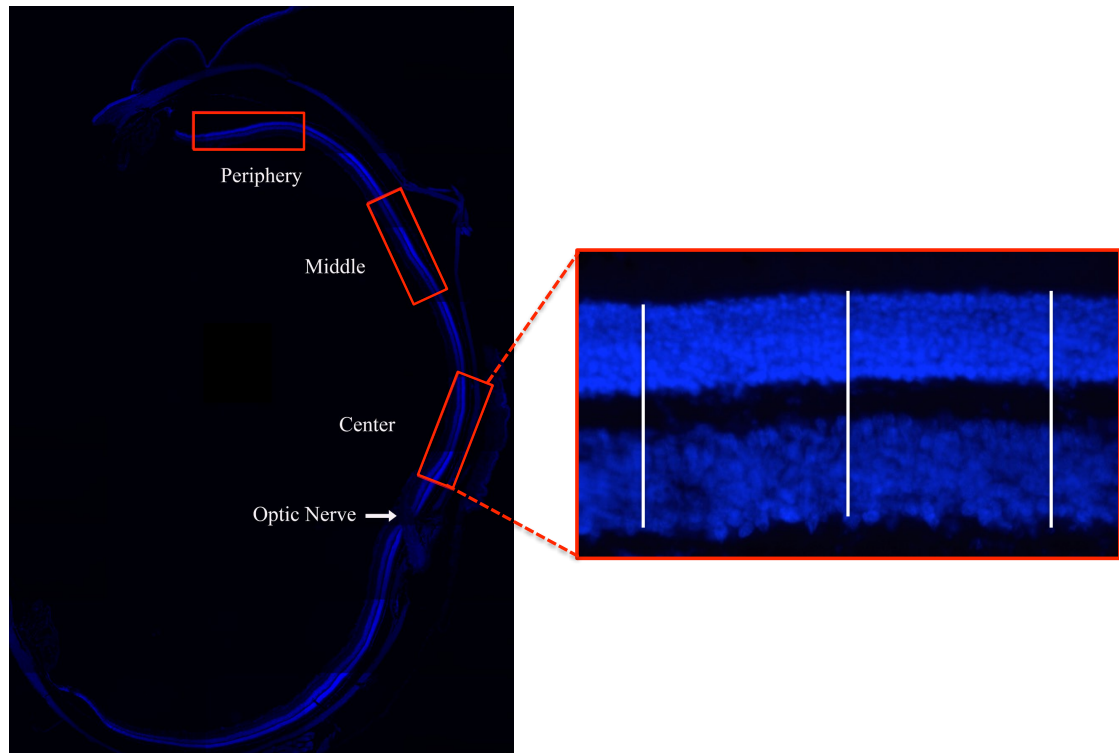


Figure 3.1: Retinal cross-section measurements.

Three measurements of each retinal layer were made within each window of images taken from the periphery, middle and center. All images were captured at 20x magnification using a fluorescent microscope.

3.4B) Retinal Flat Mount

Eyes were carefully enucleated retaining a nasally oriented pigmented tissue. The cornea was punctured with a scalpel (surgical blade stainless, No.11, Feather Safety Razor Co. LTD, Osaka, Japan) before fixing the eyecup in 4% PFA for 30 minutes. After this period the lens and cornea were carefully removed and the remaining eyecup was re-immersed in 4% PFA for 15 minutes. The retina was then carefully dissected out and

oriented with a single or double triangular cut on the nasal and dorsal aspect of the retina, respectively.

In order to help flatten the isolated retinas, filter paper was laid over top (photoreceptor side against the filter paper) and once again fixed in 4% PFA overnight. Retinas were washed in PBS, blocked in 5% normal goat serum, 0.1% tween-20, 0.3% tritonX-100 and PBS for 2 hours at RT before reacting with rabbit anti-tyrosine hydroxylase (1:500) for 4 days at 4°C. Following this period, the retinas were washed again in PBS and then stained with goat-anti-rabbit (1:1000) secondary antibody for 2 days at 4°C. Lastly, a single drop of fluoromount (091M1261, Sigma-Aldrich) was applied and a glass cover slip was laid over the tissue. To provide sufficient time for slides to cure, they were laid flat overnight and sealed with clear nail polish the following day

3.5) Electroretinogram

In vivo retinal function was assessed as a function of age between groups using a full-field ERG. Animals were anesthetized with a mixture of 5:2 ketamine (Ketalean, Bimeda-MTC Animal Health, Inc., Cambridge, ONT, Canada): xylazine (X1251, Sigma-Aldrich Co., St. Louis, MO, USA) (75 mg/kg: 30 mg/kg, respectively) via intraperitoneal injection with a 26^{1/2} gauge needle (0.45mm x 13 mm, PrecisionGlide Needle, Becton Dickinson & C., Franklin Lakes, NJ, USA). Animal body temperature was maintained at 38°C using a homoeothermic electrical blanket.

After the animal was completely anaesthetized (lack of righting reflex), pupils were dilated by corneal application of 1% tropicamide (Mydriacyl, Alcon Laboratories, Inc., Fort worth, TX, USA). Active gold recording electrodes were placed in close proximity to both corneas, while 25 gauge platinum reference electrodes were placed subdermally behind each eye and a single 25 gauge platinum ground electrode was inserted in the scruff of the back. Corneal lubrication and connection with the recording electrodes was achieved by the application of tear gels (Ophthalmic liquid gel, Novartis Pharmaceuticals Canada).

Visually elicited mass potentials from the retina were recorded using the Espion E2 system (Diagnosys LLC, Littleton, MA, USA). Light stimulation, signal amplification (0.3 -300 Hz bandpass), and data acquisition are all offered by this system. Specific combinations of light intensity and frequency of stimulation are created to reveal information on retinal nerve cell activity. For instance, amacrine cell activity can be measured by comparing the amplitude and implicit time of oscillatory potentials superimposed on the B-wave under both scotopic and photopic conditions.

3.6) Statistical Analysis

Statistical significance between groups was assessed with a two-way analysis of variance (ANOVA). Post hoc analyses were performed between groups and all three time-points using a Tukey test for multiple comparisons. A confidence interval of 95% was chosen for all analyses. Graphpad Prism 6 software was used for both the two-way

ANOVA and Tukey test (Graphpad Software, Inc., La Jolla CA). Significance was set at P less than 0.05.

3.7) Subjects

ERG recordings from five healthy human subjects aged 20-28 years old were obtained for this study. This study received ethics approval from the “Health Research Ethics Board (Biomedical Panel)” of the University of Alberta (protocol #00002108). All procedures conformed to the Code of Ethics of the World Medical Association (Declaration of Helsinki) and were done with the understanding and written consent of each participant.

Chapter. 4 RESULTS

4.1) Metabolic Phenotype

4.1A) Dietary effect on fasted blood glucose

Mazuri fed NRs displayed no significant difference in fasted blood glucose (FBG) levels as a function of age or sex, having an average of 3.9 ± 0.5 mmol/L. The cutoff for hyperglycemia was set at 5.0 mmol/L (average plus two times the standard deviation). Consistent with previous reports (Chaabo et al. 2010 and Noda et al. 2010) NRs fed standard lab chow from birth spontaneously developed hyperglycemia. A higher prevalence of HG was seen in male NRs, which became hyperglycemic as early as 6 months of age. By 12 months approximately 80% of males were HG, however by 18 months the incidence was reduced to 55% (Figure 4.1B). In contrast, Prolab fed females had a lower prevalence of HG at both 12 and 18 months of age, with only 33% and 29% of animals being HG, respectively (Figure 4.1D). Two-way ANOVA analysis revealed significantly higher FBG in 12 and 18-month-old male NRs fed Prolab 2000 ($p < 0.05$), however no significant difference was found in female NRs.

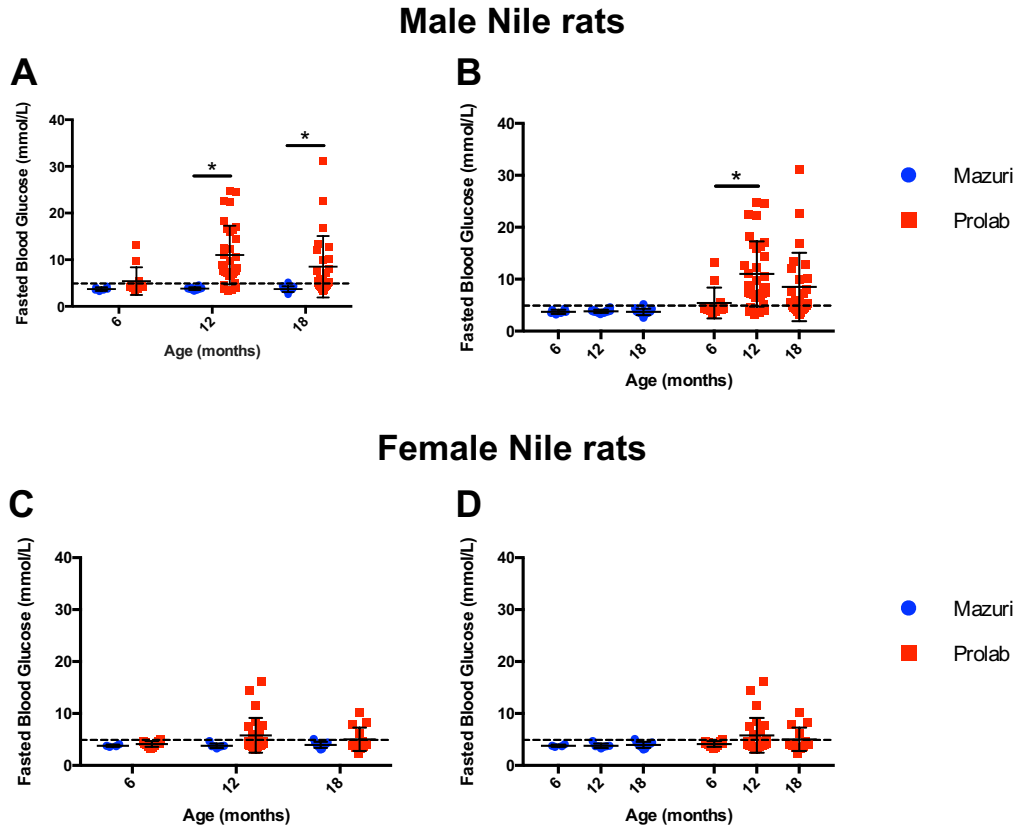


Figure 4.1: Effect of diet and age on fasted blood glucose levels.

Individual fasted blood glucose values of Mazuri (blue) and Prolab (red) fed NRs at 6mo, 12mo and 18mo. Group averages are represented by the corresponding central black line, while the black dashed line represents the cutoff for hyperglycemia at 5.0mmol/L. Neither group revealed a significant difference in FBG with aging, however male NRs revealed a significant difference between groups (F statistic 18.2, $P < 0.0001$), while female NRs did not (F statistic 3.3, $P < 0.07$). n=6-35.

* $P < 0.05$ Two-way ANOVA

4.1B) Dietary effect on glycated hemoglobin

As was observed with FBG, Mazuri fed NRs revealed no significant difference in glycated hemoglobin levels as a function of age or sex (average of $4.5 \pm 0.6\%$). Elevated HbA1c was defined as those animals with an HbA1c level greater than 6%. Consistent with FBG levels, Prolab fed NRs exhibited elevated HbA1c levels at both 12 ($7.8 \pm 1.6\%$) and 18 months ($7.7 \pm 2.0\%$), however unlike FBG there was no difference between the these time points. Comparison between groups revealed a statistically significant difference in 12 and 18 month old animals. Male and female values were not separate due to a limited number of samples.

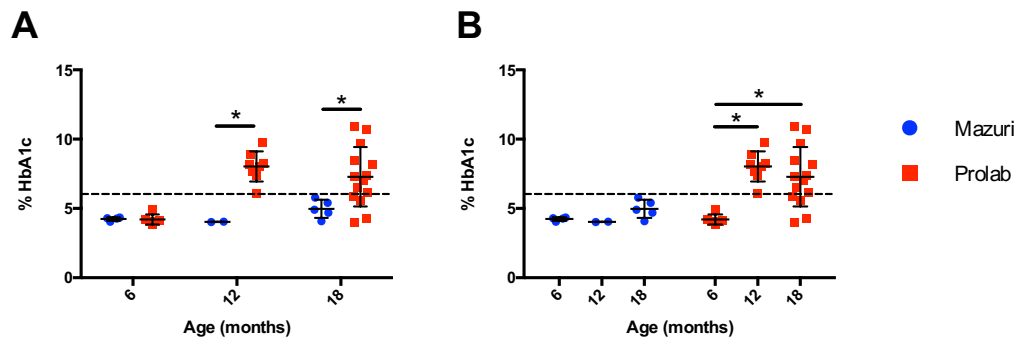


Figure 4.2: Effect of diet and age on glycated hemoglobin levels.

Individual % HbA1c values of Mazuri (blue) and Prolab (red) fed NRs at 6mo, 12mo and 18mo. Group averages are represented by the corresponding central black line, while the black dashed line represents the cutoff for hyperglycemia at 6%. A significant difference was found between the two diets at 12 and 18 months (F statistic 5.5, $P < 0.008$) and additionally revealed a significant effect of aging on Prolab, but not Mazuri fed NRs (F statistic 14.1, $P < 0.005$). $n=3-13$.

* $P < 0.05$ Two-way ANOVA

4.1C) Dietary effect on plasma insulin

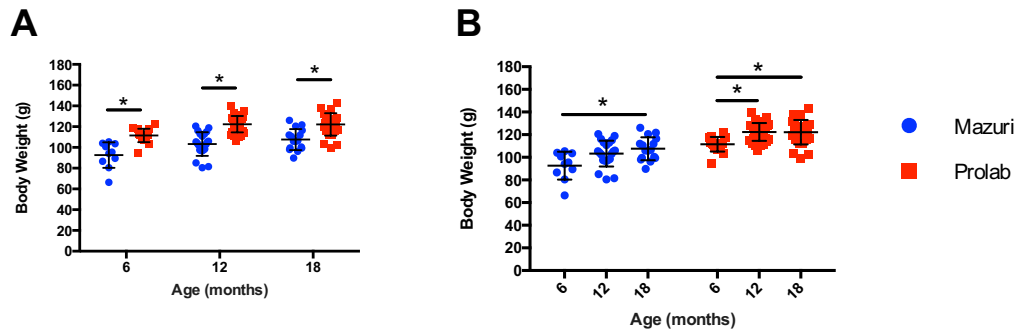
In order to further investigate the reason behind elevated FBG found in Prolab fed NRs, circulating insulin levels were measured. Mazuri fed NRs exhibited a gradual increase with aging (0.5 ± 0.3 , 2.2 ± 0.7 and 2.6 ± 0.6 ng/mL at 6, 12 and 18 months, respectively), while Prolab fed NRs exhibited a gradual decline (1.6 ± 0.9 , 0.9 ± 0.3 and 0.6 ± 0.1 ng/mL at 6, 12 and 18 months, respectively). However, two-way ANOVA analyses revealed no significant differences between the two diets or aging.

4.1D) Dietary effect on bodyweight

Further characterization of the hyperglycemic state in Prolab fed NRs consisted of bodyweight and whole body composition analysis. Male NRs reached mature size by 12 months of age with an average weight of ~ 120 g and ~ 105 g in Prolab and Mazuri fed NRs, respectively. In contrast, female NRs did not reach mature size until 18 months, having an average weight of ~ 110 g and ~ 80 g, respectively. Bodyweights were found to be statistically higher in both male (F statistic 87.1, $P < 0.0001$) and female (F statistic 55.1, $P < 0.0001$) Prolab fed NRs. Furthermore, bodyweight significantly increased in male (F statistic 14.7, $P < 0.0001$) and female (F statistic 21.2, $P < 0.0001$) NRs with age.

Echo MRI analysis of male NRs revealed greater fat and lean masses in Prolab fed NRs. Interestingly, Mazuri fed NRs showed continual accumulation of fat and lean mass up until 18 months of age, while Prolab fed animals showed no further accumulation after 12 months of age. A statistical difference was found between the two groups at all time points ($P < 0.05$).

Male Nile rats



Female Nile rats

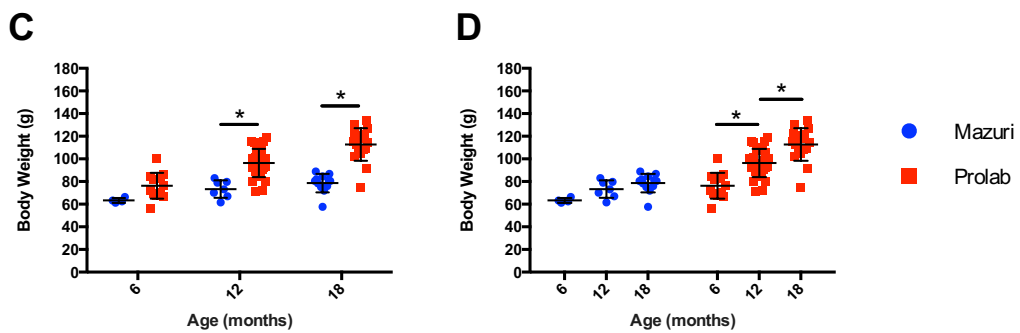


Figure 4.3: Effect of diet and age on bodyweight.

Individual body weight measurements of Mazuri (blue) and Prolab (red) fed NRs at 6mo, 12mo and 18mo. Group averages are represented by the corresponding central black line. n=9-33.

* $P < 0.05$ Two-way ANOVA

Table 2: Echo MRI Analyses

Outcome	6 month			12 month			18 month		
	Mazuri	Prolab	p-value	Mazuri	Prolab	p-value	Mazuri	Prolab	p-value
Fat (g)	14.2±4.3	22.7±3.0	<0.05	14.8±6.5	23.8±3.9	<0.05	17.4±2.0	23.0±3.9	<0.05
Fat (%)	14.6±3.7	19.4±2.2	<0.05	14.2±4.9	19.0±2.7	<0.05	15.7±3.8	18.2±2.3	ns
Lean (g)	76.6±4.6	86.3±2.5	<0.05	80.3±6.3	92.5±3.4	<0.05	82.3±5.0	93.6±4.2	<0.05
Lean (%)	79.5±3.0	74.1±2.0	<0.05	80.2±5.2	73.9±2.4	<0.05	75.5±3.2	74.4±1.6	ns

n=6-9. $P < 0.05$ Two-way ANOVA.

4.1E) Dietary manipulation of glycemic status

Nile rats were separated into two groups based on their glycemic status. Control NRs were defined as male or female Mazuri fed animals (all of which had a FBG <5.0mmol/L and HbA1c <6%). Hyperglycemic (HG) animals were defined as male or female Prolab fed NRs with a FBG >5.0mmol/L and/or HbA1c >6%.

4.2) Retinal Vascular Analysis

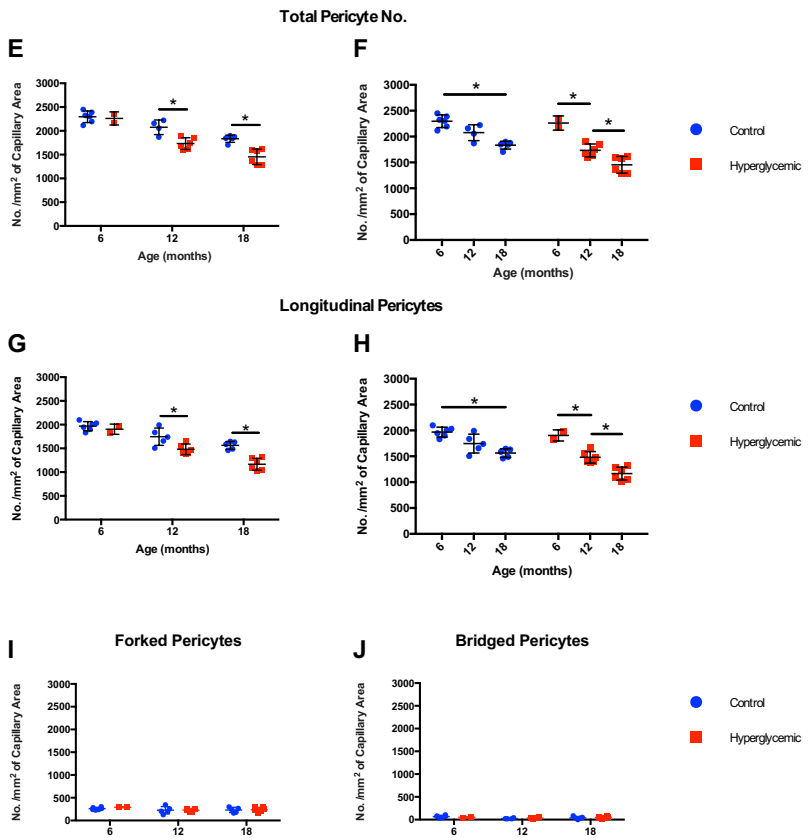
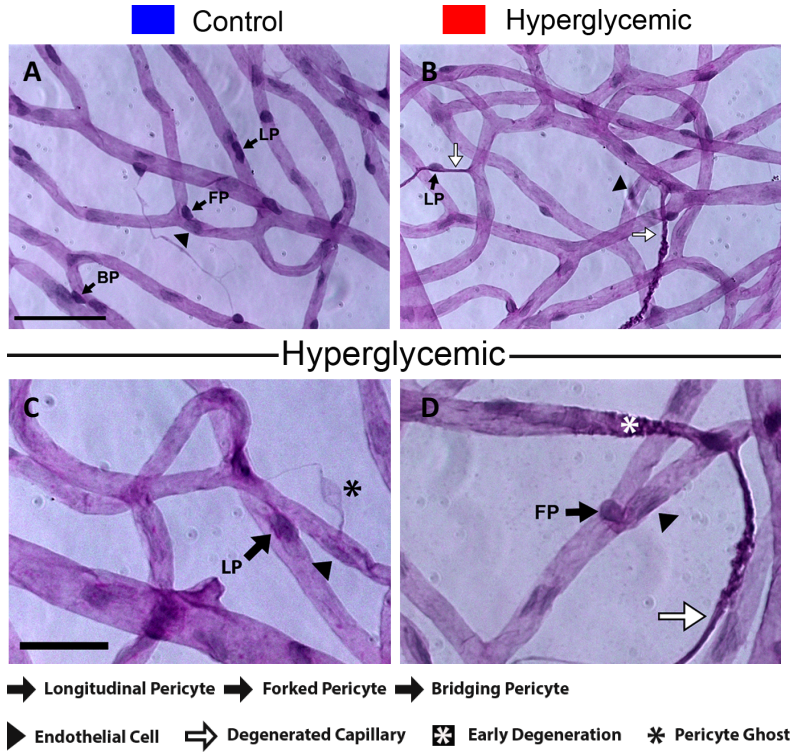
4.2A) Isolated vascular integrity

Retinal digests were performed on 6, 12 and 18month old control and HG retinas in order to observe qualitative and quantitative changes of the retinal microvasculature morphology. Two-way ANOVA analysis revealed a decline in the number of pericytes of both groups with aging (F statistic 45.7, $P < 0.0001$), however a significantly greater reduction was seen in HG retinas (F statistic 23.0, $P < 0.0001$).

Pericyte numbers were reduced by 20% in control retinas with aging (2296±93 cells/mm² at 6mo to 1833±51 cells/mm² at 18mo) compared to a 36% reduction (2262±97 cells/mm² at 6mo to 1453±144 cells/mm² at 18mo) in HG retinas (Figure 4.4E). There was a statistically significant lower number of pericytes in HG retinas compared to controls at both 12 and 18months ($P < 0.05$ and $P < 0.005$, respectively). Furthermore, pericyte loss was preferential to longitudinal pericytes (F statistic 25.1, $P < 0.0001$), while forked and bridging pericytes were spared (Figure 4.4I, J). Vascular abnormalities resembling pericyte ghosts were observed in HG retinas at both 12 and 18months, however they were not detected in controls (Figure 4.4C). Endothelial cells displayed a similar decline to pericytes as a function of aging. Control retinas had a 19.5% reduction (2772±183 cells/mm² at 6mo to 2231±50 cells/mm² at 18mo), while HG retinas were reduced by 17.5% (2634±104 cells/mm² at 6mo to 2179±200 cells/mm² at 18mo), revealing no statistically significant difference between the two groups.

The ratio of pericyte-to-endothelial cells (P: EC) in controls displayed no significant changes with age, while HG retinas revealed a decrease at 18months (Figure 4.4K, L). Comparison between groups revealed a statistically significant lower ratio in 18mo HG retinas (F statistic 15.9, $P < 0.0006$).

The number of degenerated capillaries increased in both groups with aging, however a significant increase was only seen in HG retinas. By 18 months a statistical difference was found between control (47±21 DC/mm²) and HG (132±39 DC/mm²) retinas (F statistic 8.8, $P < 0.006$). Additionally, HG retinas revealed early signs of capillary degeneration (Figure 4.4D), which was not seen in control retinas.



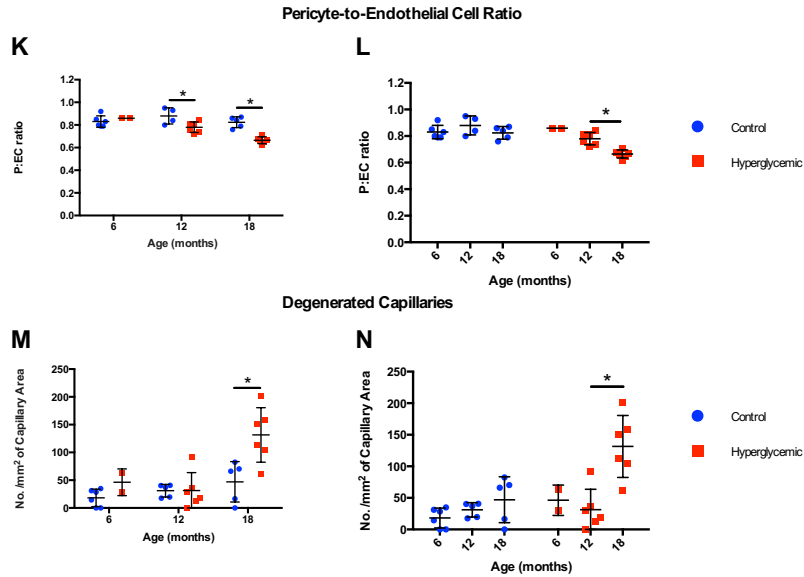


Figure 4.4: Retinal digest preparations of control and HG retinas.

Representative images of control (A) and hyperglycemic (B-D) isolated retinal vasculature stained with PAS and hematoxylin. Total pericyte number as a function of glycemia (E) and age (F), pericyte distribution as a function of glycemia (G, I, J) and age (H), pericyte-to-endothelial cell ratio as a function of glycemia (K) and age (L) and number of degenerated capillaries as a function of glycemia (M) and age (N). Scale bar in panel A=50 μ m and also applies to panel B, panel C=20 μ m and also applies to panel D. n=2-6.

* $P < 0.05$ Two-way ANOVA

4.2B) In vivo vascular integrity

Fluorescein angiography (FA) was performed in both groups of 6, 12 and 18month old NRs in order to assess the inner retinal vasculature, in vivo. Imaging of controls revealed no notable changes as a function of age, where as imaging of HG retinas was limited due to cataract formation. Cataracts were found only in HG animal's older than 12months, with increased incidence and severity as a function of age and degree of hyperglycemia. The prevalence of cataracts was greater in male NRs compared to female NRs. Cataract formation began as focal capsular cataracts (Figure 4.5A), progressing over-time to larger cataracts encompassing the entire lens by 18months (Figure 4.5E). Furthermore, a single microaneurysm was detected in the temporal-dorsal aspect of an 18month HG retina (Figure 4.6).

The number of primary vessels exiting the optic disk was quantified in order to determine if the glycemic status could be predicted through FA. Controls did not differ appreciably from 6 to 18months, displaying an average of 13 ± 1 vessels (Figure 4.7). In contrast, HG retinas revealed a gradual increase from 6 to 18months with 13 ± 0 , 14 ± 1 and 17 ± 1 at 6mo, 12mo and 18mo's, respectively. Two-way ANOVA analysis revealed significantly greater number of vessels at 18 months, however no significant difference was found with aging. Due to the low incidence of hyperglycemia at 6months, only 2 retinas were imaged.

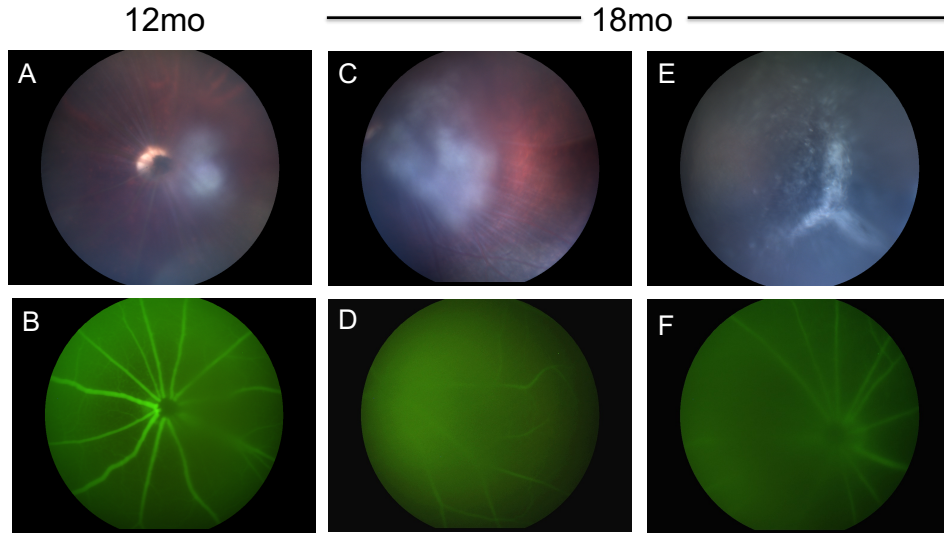


Figure 4.5: Progressive cataract development in hyperglycemic NRs.

Representative images of A) mild focal cataract and B) corresponding FA fundus image. C) Example of a more severe focal cataract and D) corresponding FA fundus image. Lastly, a diffuse cataract (E) encompassing the whole lens and F) corresponding FA fundus image.

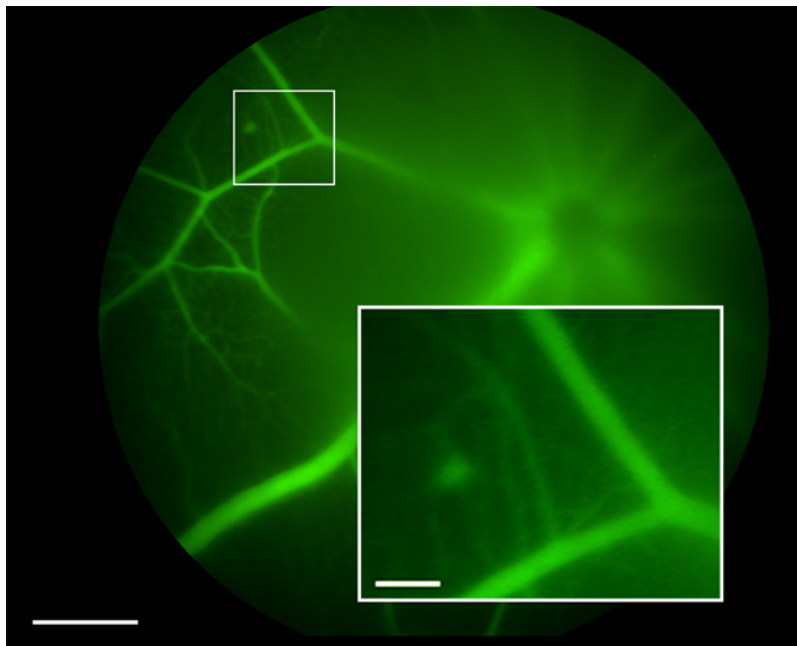


Figure 4.6: Example of a capillary microaneurysm.

A single microaneurysm was found in the temporal-dorsal aspect of an 18month HG left eye. Scale bars 200 μ m (left) and 50 μ m (right).

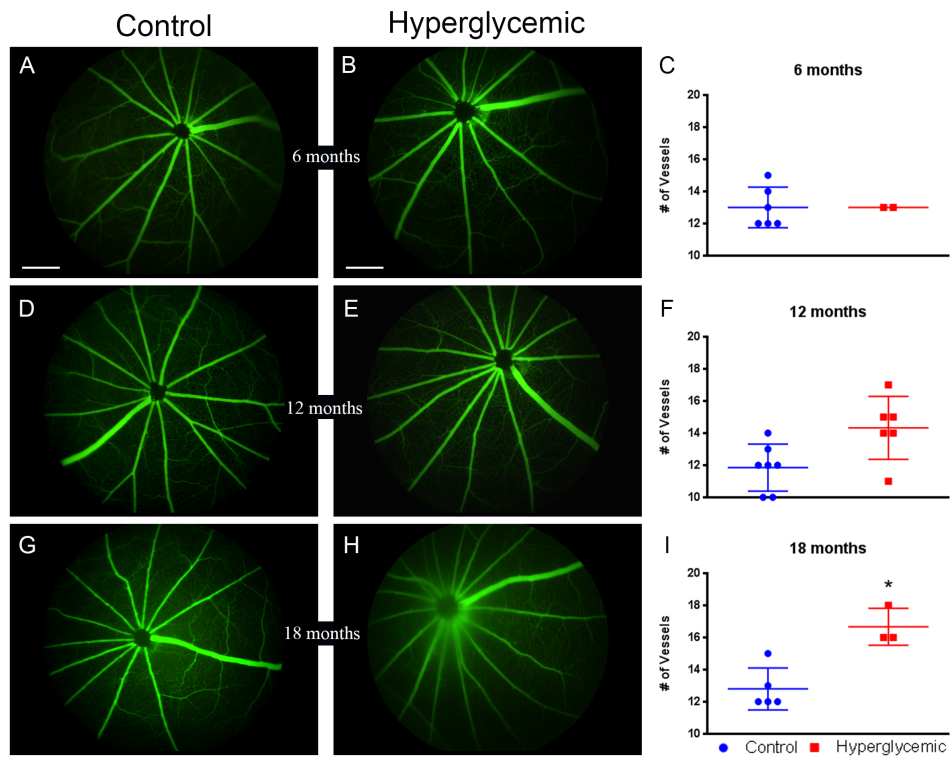


Figure 4.7: Representative fluorescein angiography fundus images.

Comparison of total primary vessel number between control (A,D,G) and hyperglycemic (B,E,H) retinas at 6mo (C), 12mo (F) and 18mo (I). n=2-6.

Scale bars in panel A-B: 200 μ m

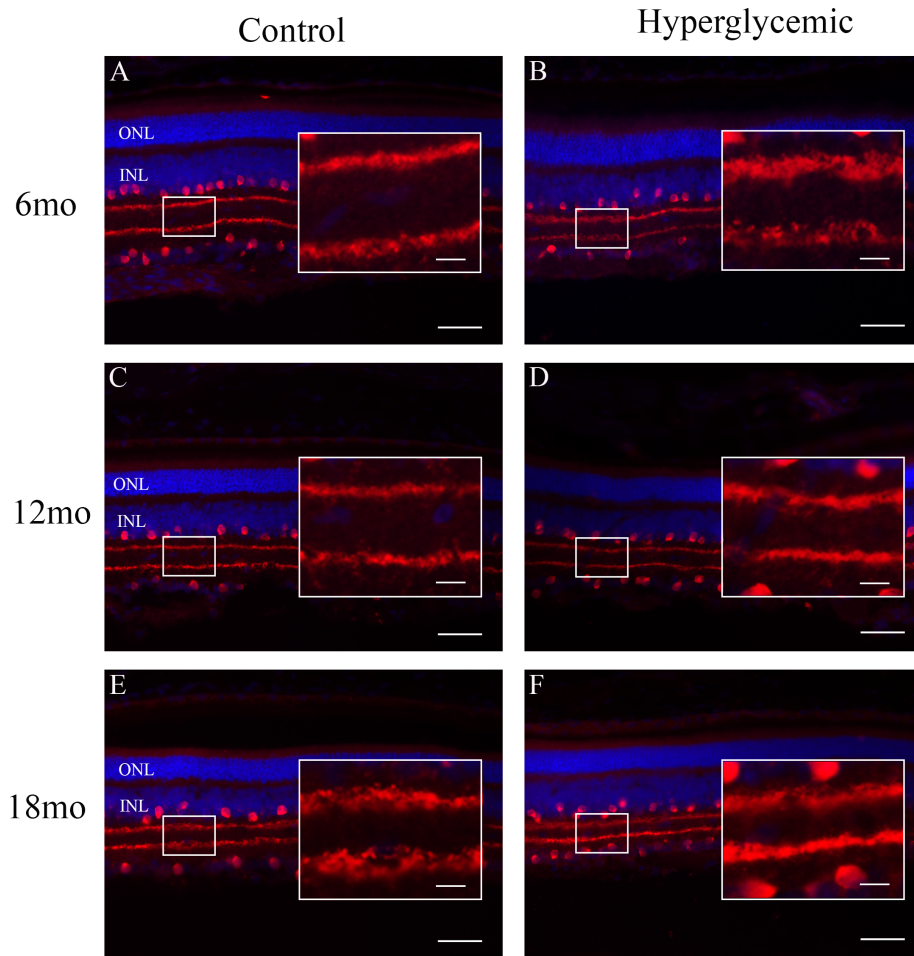
* $P < 0.05$ Two-way ANOVA

4.3) Retina Cross-sectional Staining

4.3A) Amacrine cells

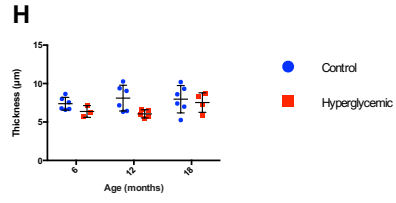
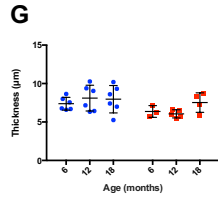
Amacrine cell dysfunction (as indicated by a loss of ERG oscillatory potentials) is widely accepted as an early marker of DR, however it has yet to be identified which subtypes of amacrine cells are affected. Here we investigate two types of amacrine cells: 1) cholinergic labeled with anti-choline acetyl transferase (ChAT) and 2) dopaminergic label by anti-tyrosine hydroxylase (TH) in order to assess any anatomical changes.

Consistent with previous reports (Liets et al. 2006) in humans, anti-ChAT staining revealed two layers of amacrine cell bodies and dendrites: 1) one layer of amacrine cell bodies was found in the INL, with a corresponding dendritic layer in sublamina –a (outer) of the IPL. 2) A second layer of amacrine cell bodies was found in the GCL, again with a corresponding dendritic layer in sublamina –b (inner) of the IPL (Figure 4.8). No significant differences were found in the dendritic layer thickness of sublamina –a or -b as a function of age in control and HG retinas at all eccentricities (Figure 4.8).

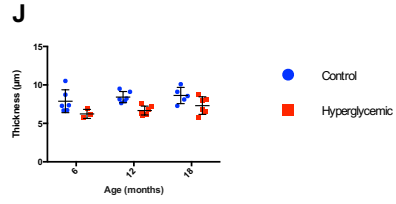
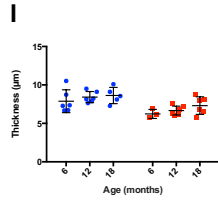


Sublamina -a

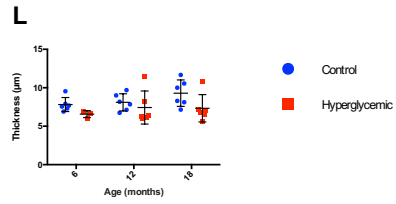
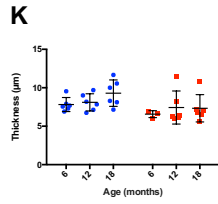
Periphery



Middle



Center



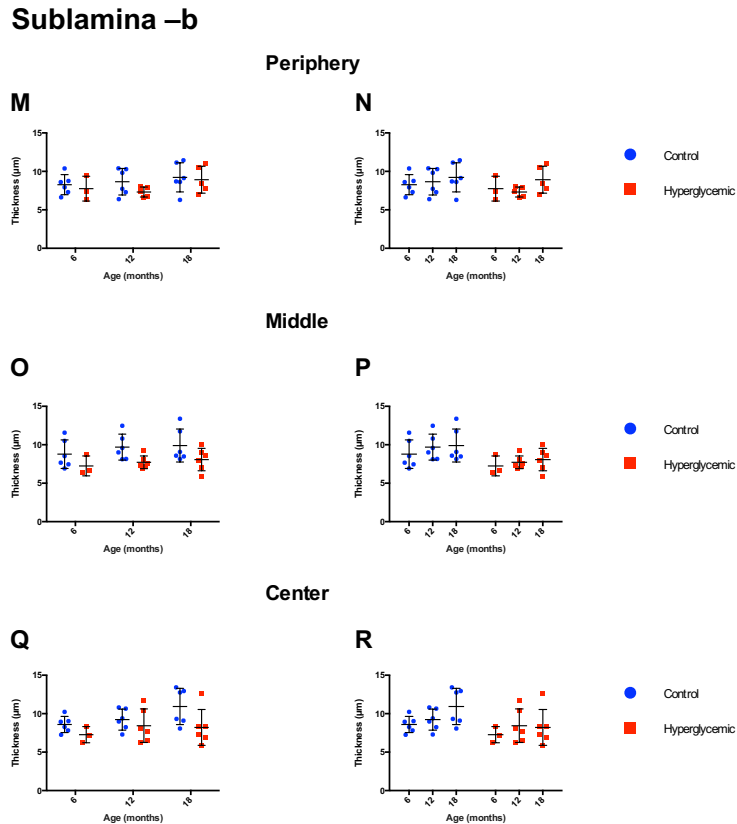


Figure 4.8: Cross-sectional analysis of cholinergic amacrine cells.

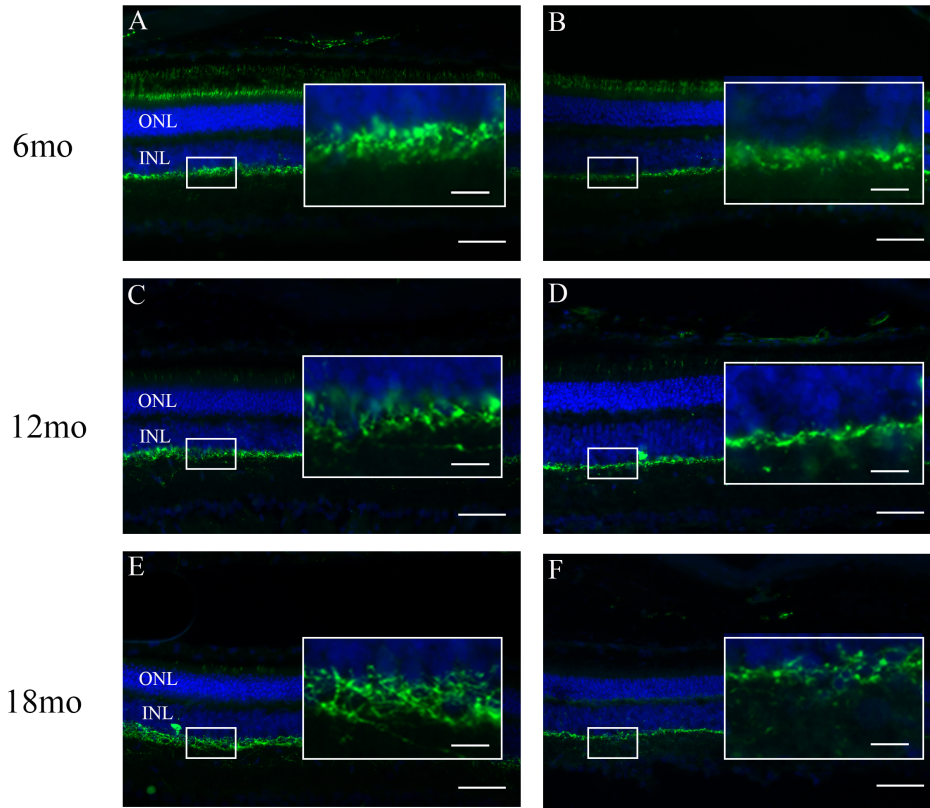
Retinal cross-sections stained with anti-ChAT from 6month (A, B), 12month (C, D) and 18month (E, F) of control (left) and hyperglycemic (right) retinas.

Comparison of the dendritic layer thickness of sublamina -a at the periphery (G, H), middle (I, J) and center (K, L) of the retina. Comparison of the dendritic layer thickness of sublamina -b at the periphery (M, N), middle (O, P) and center (Q, R) of the retina Scale bars –main image 50µm, enlarged inset 10µm. Outer nuclear layer (ONL), inner nuclear layer (INL). n=6.

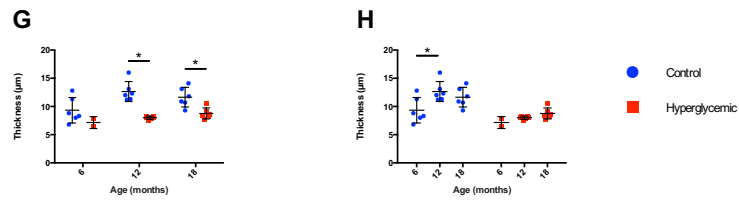
Similar to cholinergic amacrine cells, dopaminergic amacrine cell bodies were found in 2 layers: the INL and less frequently in the GCL (Figure 4.9). However, compared to cholinergic far fewer dopaminergic cell bodies were seen in both layers and only a single dendritic layer was found in sublamina -a of the IPL. Additionally, the dendritic layer of controls displayed a thicker gradient towards the center of the retina with aberrant fiber growth as a function of age at all eccentricities. On the other hand, HG retinas did not exhibit fiber growth with aging and dendritic densities were reduced across all eccentricities. Two-way ANOVA multiple comparisons revealed significantly thicker dendritic layers in control retinas of 12 and 18-month-old NRs and as a function of age (Figure 4.9). Layers were normalized against the ONL and INL to control for any potential artifact of oblique sectioning, however this revealed no difference from the absolute values (not shown).

Control

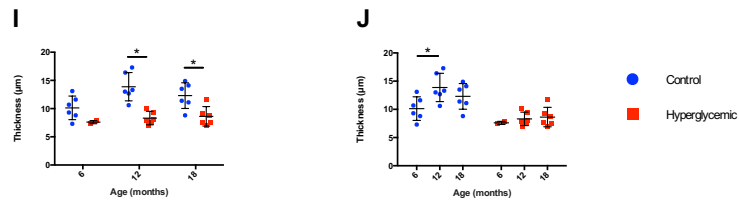
Hyperglycemic



Periphery



Middle



Center

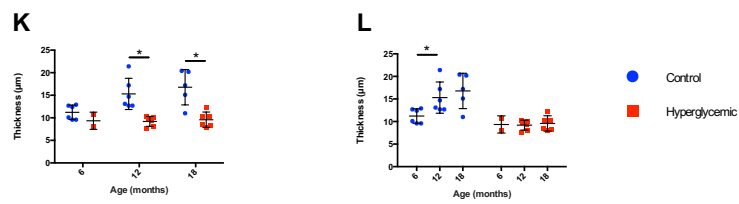


Figure 4.9: Cross-sectional analysis of dopaminergic amacrine cells.

Retinal cross-sections stained with anti-TH from 6month (A-B), 12month (C-D) and 18month (E-F) of control (left) and hyperglycemic (right) retinas.

Comparison of the dendritic layer thickness between NG and HG retinas. Scale bars –main image 50 μ m, enlarged inset 10 μ m. Outer nuclear layer (ONL), inner nuclear layer (INL). n=6.

* $P < 0.05$ Two-way ANOVA

4.3B) Connexin 36

Patients with DR have reported reduced night vision in the earliest stages of the disease, however the underlying mechanism is not known. Demb et al. 2002 suggests an essential role of the gap junction connexin 36 (Cx36) for scotopic vision. Here we investigate Cx36 expression in control and HG retinal cross-sections, using confocal microscopy. Control retinas of all ages revealed 2 primary layers of staining: a single band in the OPL and punctate staining in the IPL. In contrast, 18month HG retinas exhibited less staining in both layers. Furthermore, reduced staining corresponded with the extent of hyperglycemia. Severely hyperglycemic (31.2mmol/L) retinas (Figure. 4.10C) exhibited less staining compared to mildly hyperglycemic (8.0mmol/L) retinas (Figure. 4.10B), which had less staining than control (4.1mmol/L) retinas (Figure. 4.10A).

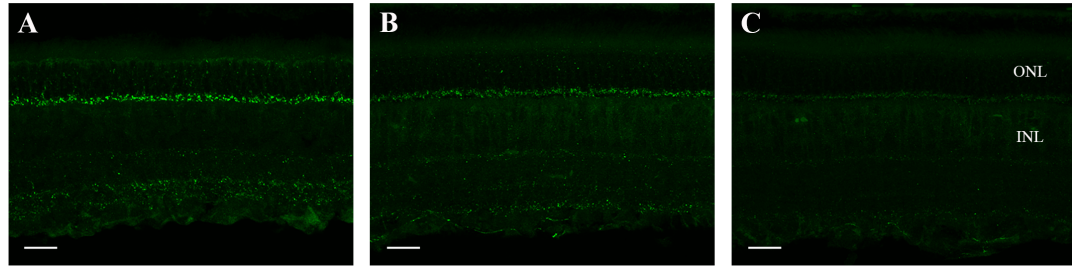


Figure 4.10: Effect of hyperglycemia on Cx36 expression.

Representative confocal images of Cx36 in 18 month A) normoglycemic – 4.1mmol/L, B) mildly hyperglycemic – 8.0mmol/L and C) severely hyperglycemic – 31.2 mmol/L retinas. Scale bar 20 μ m. Images were taken by Sharee Kuny. n=3.

4.3C) Connexin 43

The predominant morphological changes seen in the early stages of DR are a loss of pericytes surrounding the capillaries, however the mechanism that leads to pericyte loss is still unknown. A recent review (Winkler et al. 2011) of pericyte/endothelial cell interactions describes a fundamental role of connexin-43 (Cx43) for stable pericyte/endothelial cell interaction. Here we investigate the expression of Cx43 in retinal cross-sections using confocal microscopy. Control retinas (Figure 4.11A) from 18month NRs revealed organized staining around the inner retinal vasculature. Age-matched mildly hyperglycemic (8.0mmol/L) retinas (Figure. 4.11B) displayed similar staining pattern as control retinas, however severely hyperglycemic (31.2mmol/L) retinas (Figure. 4.11C) showed aggregates of staining that was no longer surrounding blood vessels.

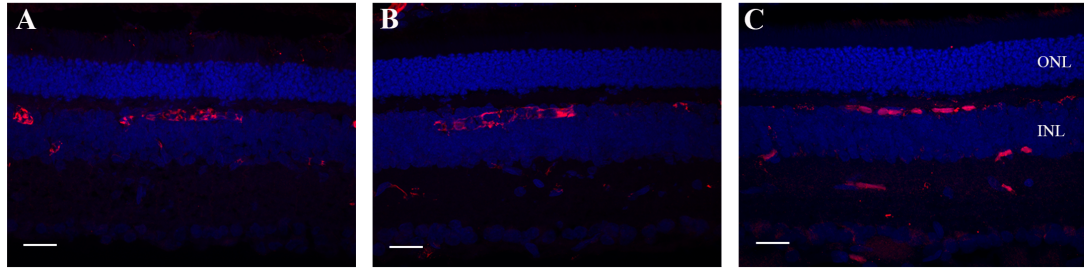


Figure 4.11: Effect of hyperglycemia on Cx43 expression.

Representative confocal images of A) normoglycemic B) mildly hyperglycemic and C) severely hyperglycemic 18month old retinas. Scale bar 20 μ m. Images were taken by Sharee Kuny. n=3.

4.3D) Glial Fibrillary Acidic Protein

In response to retinal stress/injury, Müller glial cells accumulate glial fibrillary acidic protein (GFAP). STZ-induced models of DR have reported elevated expression of GFAP, despite reports of both elevated and unaltered levels of GFAP in human DR samples. Retinal cross-sections were stained with GFAP and imaged using confocal microscopy. Both control and HG retinas exhibited prominent staining in the end feet of Müller cells, with light staining of processes extending towards the outer retina. The peripheral retina (not shown) displayed a greater amount of process staining compared to the central retina (Figure 4.12A-C), due to mechanical stress. No notable differences were seen between the two groups at all time points.

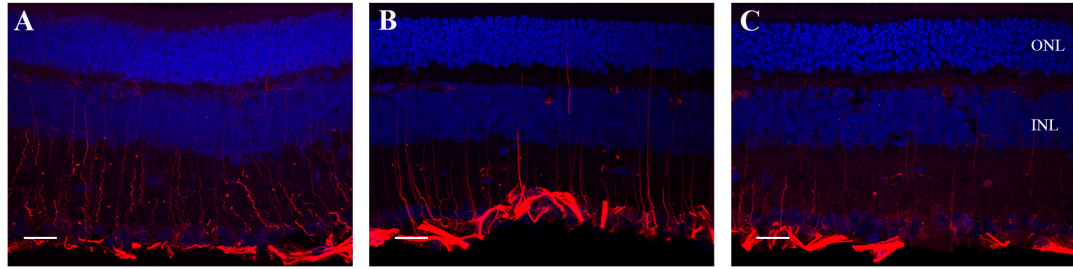


Figure 4.12: Effect of hyperglycemia on GFAP expression.

Representative confocal images of GFAP in A) normoglycemic B) mildly hyperglycemic and C) severely hyperglycemic 18month old retinas. Scale bar 20 μ m. Images were taken by Sharee Kuny. n=6.

4.3E) Tomato Lectin

In order to characterize the microvascular anomalies of the inner retina, retinal cross-sections were stained with tomato lectin and imaged using confocal microscopy. Control retinas revealed no discernable distinction between age or eccentricity of the retina. In contrast, 18 month HG retinas displayed regions of tortuosity not seen in age-matched control retinas (Figure 4.13C). These regions of tortuosity may be linked to reduced pericyte numbers and subsequent lack of structural support.

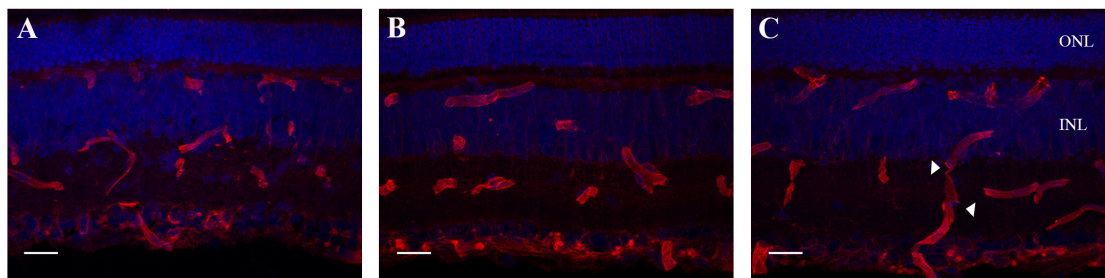


Figure 4.13: Effect of hyperglycemia on inner retinal vasculature morphology.

Representative confocal images of tomato lectin staining of A) normoglycemic B) mildly hyperglycemic and C) severely hyperglycemic 18month old retinas. Arrowheads indicate sites of tortuosity. Scale bar 20 μ m. Images were taken by Sharee Kuny. n=6.

4.3F) Retinal Flat Mount

Previous studies (Gastinger et al. 2006) have reported a reduced number of dopaminergic and cholinergic amacrine cell bodies in diabetic retinas. Retinal flat-mounts were performed on 5x 18month control retinas and stained with anti-TH as a proof of principle for counting cell bodies. An average of 31 ± 3 cell bodies/ mm^2 was found. Due to limited availability of retinas no comparisons were made between groups, however future investigations will be able to follow the provided protocol (see methods) in order to research this area further.

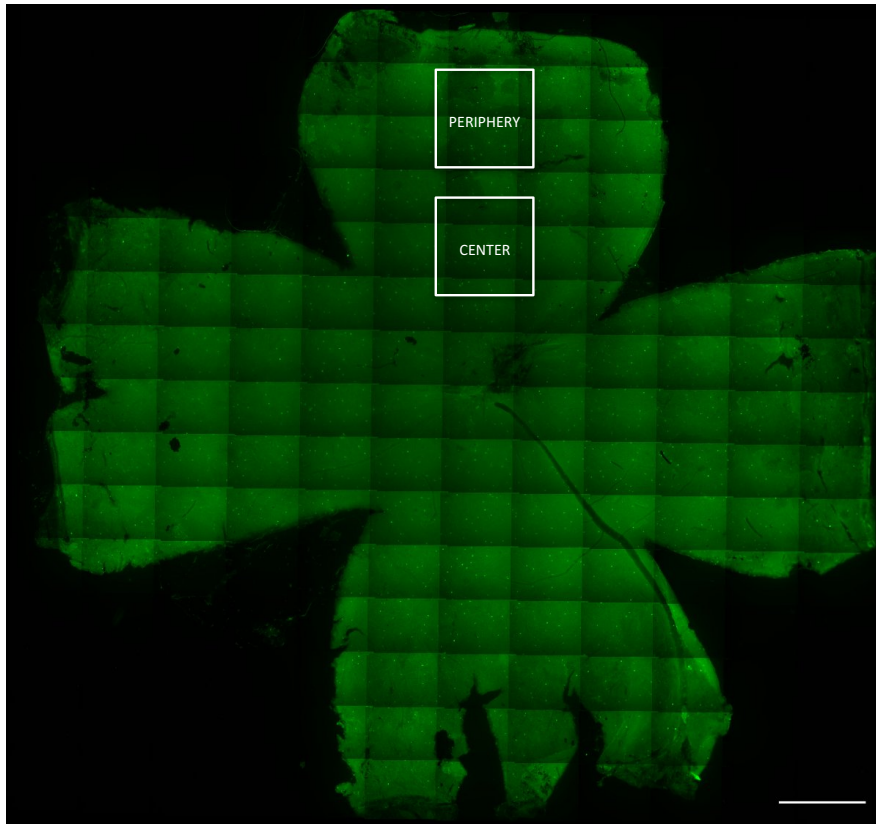


Figure 4.14: Example of retinal flat-mount stained with anti-TH.

Cell bodies were counted at both the periphery and center of each quadrant of the retina. Dorsal – 2 slits, nasal – 1 slit. Scale bar 1000 μ m

4.4) Electroretinogram

4.4A) Anesthesia

Initial ERG recordings were undertaken in NRs anesthetized with a 5:1 ratio of ketamine: xylazine (75mg/kg: 15mg/kg). However, inconsistency in depth and time to sedation prompted an increase in xylazine dosage to 30mg/kg. As a result NR sedation was more rapid and consistent. Unfortunately, a large portion HG Nile rats (12months or older) died from the anesthetic, precluding comparison between the two groups at these

time points. For this reason, no quantifiable comparisons of ERG recordings were made between the two groups.

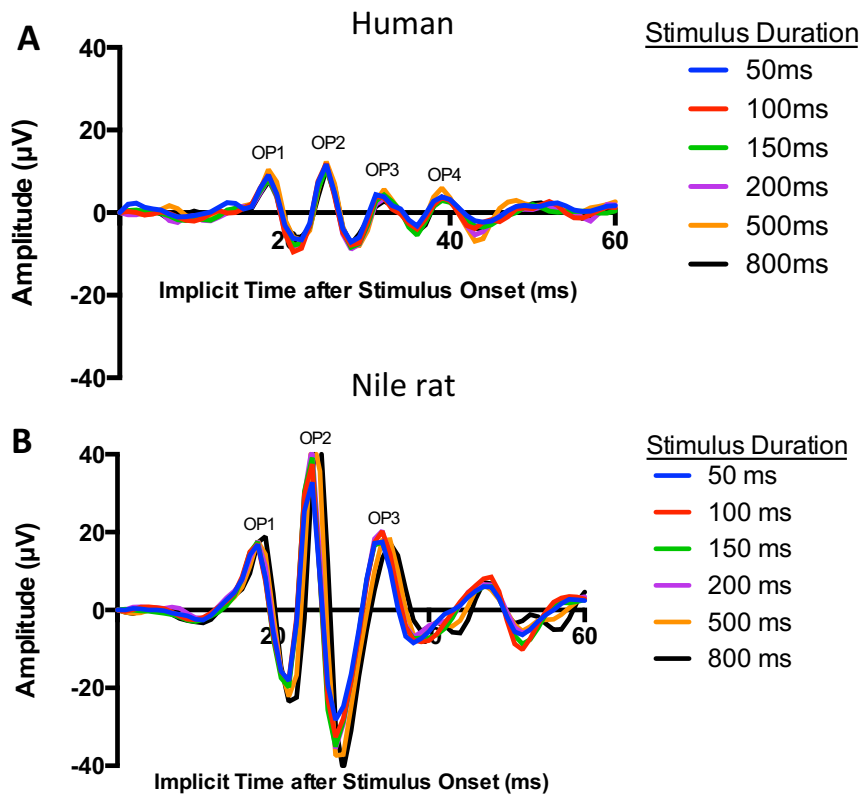
In light of the number of anesthesia related deaths, ketamine: xylazine was substituted for isoflurane inhalation anesthesia (SomnoSuite®, Kent Scientific co.). Preliminary trials on six 18month HG Nile rats resulted in zero deaths and viable ERG traces (not shown). This will allow future investigation of functional differences between control and HG retinas.

4.4B) Comparison between human and Nile rat oscillatory potentials

To further investigate the relevance of the NR as a model to recapitulate human vision, we compared properties of the cone-driven ON- and OFF- pathways to humans. OPs were specifically chosen for investigation, as reduced OPs have been reported in human DR. Time and amplitude of the ON (b-wave) and OFF (d-wave) OP components were assessed in 5 human subjects (aged 20-40 years; recordings taken by Dr. Ioannis Dimopoulos) and 5 NRs (aged 2-6 months). Under 30 cd/m² background adaption, a white stimulus (intensity of 2.75 log cd•s/m²) was presented at durations increased in a stepwise fashion from 10ms to 800ms in eight steps. A total of 20 traces were averaged at each step and individual oscillatory potentials were analyzed with trough-to-peak measurement from traces filtered at 75-300Hz bandpass.

Humans displayed four distinct OP peaks that were phase-locked to the ON response (ON-OPs). The ON-OPs (OP1-4) timing remained constant for all stimulus durations (peaks at t=19ms, t=25ms, t=32ms and t=40ms after stimulus onset) with amplitudes also remaining constant after stimuli durations >20ms (Figure 4.15A). For the OFF phase, two distinct OPs were distinguished. OFF-OPs (OP1-2) timings remained

constant for stimuli durations >100ms (peaks at $t=19\text{ms}$ and $t=26\text{ms}$ after stimulus offset). Nile rats displayed three distinct OP peaks that were phase-locked to the ON response (Figure 4.15B). As with humans, timing remained constant for all stimulus durations (peaks at $t=20\text{ms}$, $t=27\text{ms}$ and 39ms). However, contrary to humans, the amplitude of the ON-OPs increased as a function of stimulus duration (Figure 4.15C). For the OFF phase, two distinct OPs were also distinguished. The timing of the OFF-OPs was reduced as a function of stimulus duration. For both ON and OFF responses, OP peaks (from filtered traces) preceded the peaks from raw traces by 1-2ms.



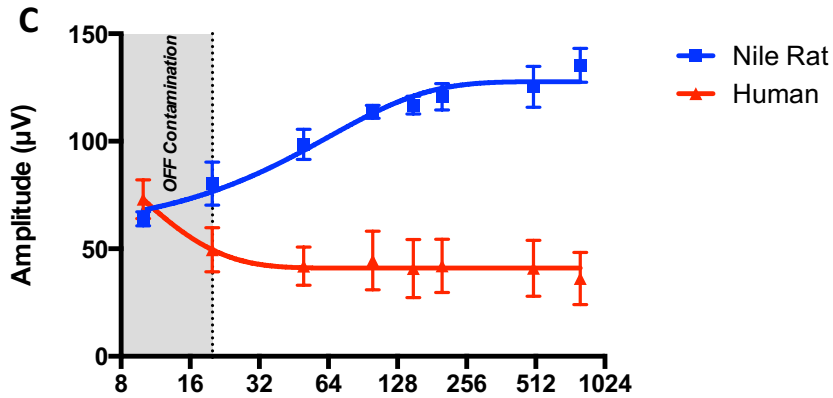


Figure 4.15: Comparison of filtered human and NR ON-OPs.

Amplitude and implicit time of human (A) and NR (B) ON-OPs as a function of stimulus duration. OP implicit time was consistent in human and NRs amongst increasing stimulus duration, however NRs showed a slight increase in the amplitude of OP1 and OP2. Summated amplitudes of ON-OPs in both human and NRs is shown in panel C. Following separation of the ON- and OFF- components NRs exhibit amplitude growth as a function of stimulus duration, however humans showed no changes. n=6-9.

Chapter. 5 DISCUSSION

5.1) Glycemic status

Weir et al. 2004 has proposed a five-stage model for the progression of diabetes. Each of the stages is characterized by changes in β -cell mass and function, insulin secretion and circulating glucose concentrations. Stage 1 (compensation) occurs when insulin secretion is increased to maintain normoglycemia in insulin resistant individuals. Insulin resistance may occur for a number of reasons, such as increased adiposity, lack of exercise and genetic predisposition. Progression into stage 2 (stable adaptation) transpires, as a loss of β -cell mass and subsequent β -cell function induces in a gradual rise of glucose levels. Stage 3 (unstable early decompensation) is characterized by further β -cell dysfunction and rapid rise in glucose levels to reach stage 4 (stable decompensation). Finally, stage 5 (severe decompensation) represents a profound reduction in β -cell mass and insulin secretion with progression to ketoacidosis from excessive fat degradation.

Consistent with previous findings (Noda et al. 2010 and Chaabo et al. 2010), NRs fed standard lab chow followed a similar progression of diabetes. According to the conditions of the five stages, we found that 6-month-old NRs exhibited features of stage 1 and 2 with progression to stages 2-5 by 12 months of age. Interestingly, by 18 months of age there was a reduction in both FBG and insulin levels, suggesting a potential sixth stage that is characterized by a return to baseline glucose and insulin levels. Investigation of glycated hemoglobin levels revealed similar high levels at both 12 and 18 months of age, signifying the 18-month-old NRs were previously HG. A potential explanation for the drop in FBG levels could be due to the development of hepatic and abdominal tumors

that were often observed in 18-month-old NRs with low circulating glucose levels. Iglesias et al. 2014 demonstrated that tumors and liver-tumor infiltrations will consume excess glucose, which could result in lower FBG levels. Additionally, preliminary studies from metabolic cages indicated a reduction in appetite that could further contribute to reduced FBG levels. Loss of appetite is often observed in individuals with tumors (Solheim et al. 2014), further supporting the likelihood of tumor-induced reduction of FBG levels. Future studies may investigate the reduction in FBG through longitudinal measurements, as HbA1c can only provide an approximation of the previous 3 months. Furthermore, Dr. Consolato Sergi is currently investigating the relationship between HG and hepatic-tumor development, which could provide further insight into this paradigm.

Mazuri fed NRs (controls) remained in stage 0 (normal) up to 12 months of age, at which point a slight shift to stage 1 began. No further progression past stage 1 was found at 18 months of age, as indicated by normoglycemia with slight hyperinsulinemia. These findings suggest that dietary intervention was sufficient to prevent the onset of HG in NRs, however if given enough time they could go on to develop HG.

Sexual dimorphism of hyperglycemia has been reported in both human and animal models of DM (Kava et al. 1989). The present study confirms these findings in NRs, in which a higher incidence and degree of hyperglycemia was found in male NRs. Classically, it has been postulated that higher estrogen levels in females may be protective against hyperglycemia (Le May et al. 2006). Although, we cannot rule out the protective role of estrogen, preliminary studies involving metabolic cages also revealed greater activity in female NRs. We propose that the additional physical activity exhibited by female NRs may account for the reduced incidence and severity of HG. The beneficial

effects of exercise on diabetes prevention are well document, however an additional question still remains, why are female NRs more active? Further investigation into the relationship between circadian rhythm and development of HG may provide further insight into the development of T2DM.

Blood glucose monitoring is the primary tool used to manage diabetes. This is achieved by applying a single drop of blood to the testing strip of a glucose meter. Depending on your age, duration of diabetes, known complications and individual consideration, certain target ranges can be determined (Diabetes.org). The present study used a single FBG measures in order to determine the glycemic status of the animal. Consistent methodology and minimal animal handling is essential for reliable FBG measurements. All measurements must be assessed prior to injection of any anesthetic or other pharmacological agents, which will cause an increase in FBG levels. Furthermore, allowing 30minutes for the animal to acclimatize to the experimental room and also minimal handling of animal will reduce any stressed induced inflation of FBG levels. A single Mazuri fed NR had a portion of hair removed from its inner thigh in order to expose the saphenous vein and obtain a drop of blood. The procedure took approximately 15minutes and the FBG measurement was surprisingly high, at 10.2mmol/L. This value was considered artificially high due to inconsistency with previous measurements in Mazuri fed NRs and stress of the procedure. Lastly, in order to further understand the pathogenesis of diabetes complications, it is essential to monitor FBG levels longitudinally. This will help determine of the sequence of events that occur in relation to duration of HG.

5.2) Effect of Hyperglycemia on the Retina

5.2A Pericyte loss

Cogan et al. (1879) first identified pericyte loss as an early pathological feature of DR, which preceded microaneurysm formation and microvascular leakage. While current rodent animal models of DR do not recapitulate all of the features of human DR, the majorities do exhibit some degree of pericyte loss. However, the limitation of these rodent animal models stems from their amount of retinal pericyte coverage. A healthy human retina contains a 1:1 ratio of pericyte-to-endothelial cells, while mice and rats retinas have a substantially lower ratio of about 1:3. In contrast, NRs exhibit similar pericyte coverage to humans, with just under a 1:1 ratio in healthy young animals. This gives the NR animal model a considerable advantage over current animal models to undertake studies concerning pericyte loss.

In the present study, we investigated the effect of both aging and HG on retinal pericyte coverage. Our results confirmed HG-related pericyte loss, but contrary to previous studies in rats (Hughes et al. 2006) also revealed an age-related decline in pericyte number. The discrepancy found between the two studies could be explained by a few possibilities. First, as mentioned earlier NRs contain a greater number of pericytes compared to rats, which could suggest an age-related susceptibility to pericyte loss. Secondly, pericyte cell bodies were labeled by different methods in the two studies. The present study used classical PAS and hematoxylin staining to label pericytes and endothelial cells, where as Hughes et al. 2006 used a pericyte soma specific Ab, NG2 chondroitin sulfate proteoglycan (Chemicon). A limitation of PAS staining lies in the subjective distinction between pericytes and endothelial cells (pericytes are rounder and

stained darker, compared to oval shaped and lighter stained endothelial cells). NG2 staining on the other hand, may label some but not all pericytes, resulting in a lower overall count. Future studies could assess differences between the two methods by comparing retinal digests (from the same animal) with each method. Lastly, hyperinsulinemia seen in 18month control animals prompts the question if the age-related decline in pericyte number is due to aging alone. Future studies may address this question through exogenous insulin injections in young healthy NRs to examine the effect of hyperinsulinemia on retinal pericyte number. The outcome of such experiments would be of interest to all diabetic patients, as exogenous insulin is the primary treatment for all T1DM patients and also a large portion of T2DM patients.

Additional investigation of pericyte loss determined preferential loss of pericytes located on straight capillaries, while sparing pericytes located on forked capillaries or bridging between capillaries. Pfister et al. 2008 reported a similar specificity of pericyte loss, however the cause was unknown. A feasible explanation for this specificity can be taken from Park et al. 2014, reporting altered pericyte integrin expression in HG conditions. Park suggests that Ang2 induced pericyte apoptosis is only viable when the integrin expression is changed from $\alpha 1\beta 1$ or $\alpha 2\beta 1$ to $\alpha 3\beta 1$, which can recognize the appropriate ligands for the p53 pathway. Taken together we can infer that pericytes located on straight, forked and bridged capillaries may express different integrin's, resulting in preferential susceptibility to different conditions.

Hammes et al. 2010 suggests the progression of DR proceeds from pericyte loss to endothelial cell death and ultimately vasoregression. While our results did not show a significant reduction in endothelial cell number, HG retinas exhibiting the lowest number

of pericytes also exhibited lower than average EC count and increased number of degenerated capillaries. These results are in support of Hammes hypothesis, however we also found conflicting evidence. Retinal digests of 12 and 18month HG retinas revealed signs of early capillary degeneration, which still contained pericyte and endothelial cell bodies. Based on this evidence, it is likely that an alternative mechanism, such as microvascular occlusions, may be contributing to vasoregression. The formation of occlusions is thought to occur due to increased leukocyte adhesion, blood viscosity, platelet stickiness and aggregation of AGE, which all contributes to the formation of a clot. Insufficient downstream blood flow will eventually cause degeneration of the capillary and regions of non-perfusion.

Current theories concerning pericyte loss propose high circulating glucose levels are responsible for activating apoptotic pathways in pericytes, yet the exact pathways are still unknown (Mizutani et al. 1996). The present study confirmed a significantly greater amount of pericyte loss in HG retinas compared to age-matched controls. However, the amount of pericyte loss correlated with HbA1c levels and not FBG. In humans, as FBG levels rise so does the amount of glycated hemoglobin, however as previous mentioned (Chapter 5.1) this was not the case in the NR. NRs exhibited a decline in FBG from 12 to 18months, despite HbA1c levels remaining high. Given enough time, it would be expected that HbA1c would also decline. Based on these findings, we propose that pericyte loss is more closely coincident with HbA1c levels rather than circulating glucose levels. Figure 5.1 shows a proposed mechanism of how increased glycation of hemoglobin could contribute to pericyte loss. First, high circulating glucose levels result in increased glucose uptake by RBCs. As a result more hemoglobin become glycated and

bind oxygen more strongly, reducing the amount of oxygen delivered to tissue.

Additionally, increased glucose uptake by RBC's will further activate glycolysis and the production of secondary byproducts, such as 2,3-biphosphoglycerate, which has been shown to cause a rightward shift in the oxygen dissociation curve, preventing full oxygen saturation of hemoglobin. In combination with microvascular occlusions and degenerated capillaries, these mechanisms contribute to regions of hypoxia. It is well established that hypoxia is the primary trigger of neovascularization through HIF-1- α activation of VEGF, however the role of hypoxia in pericyte loss has yet to be established. Simon et al. 2008 describes an important relationship between HIF-1- α and Ang2 up regulation. Under normal conditions Ang1 binds to endothelial cell Tie2 receptors promoting vascular stability. In contrast, when up regulated Ang2 competitively inhibits the Tie2 receptor causing vascular destabilization and pericyte death (Hammes et al. 2004). Taken together, these two findings may explain a possible connection between hypoxia and pericyte loss.

Diabetic retinopathy is not a uniform disease in which hyperglycemia leads to the activation of a single mechanism. It is a complex multifactorial disease that activates many pathological pathways that may or may not compliment each other. For this reason, discerning the precise mechanism underlying DR pathogenesis has proven very complex and difficult.

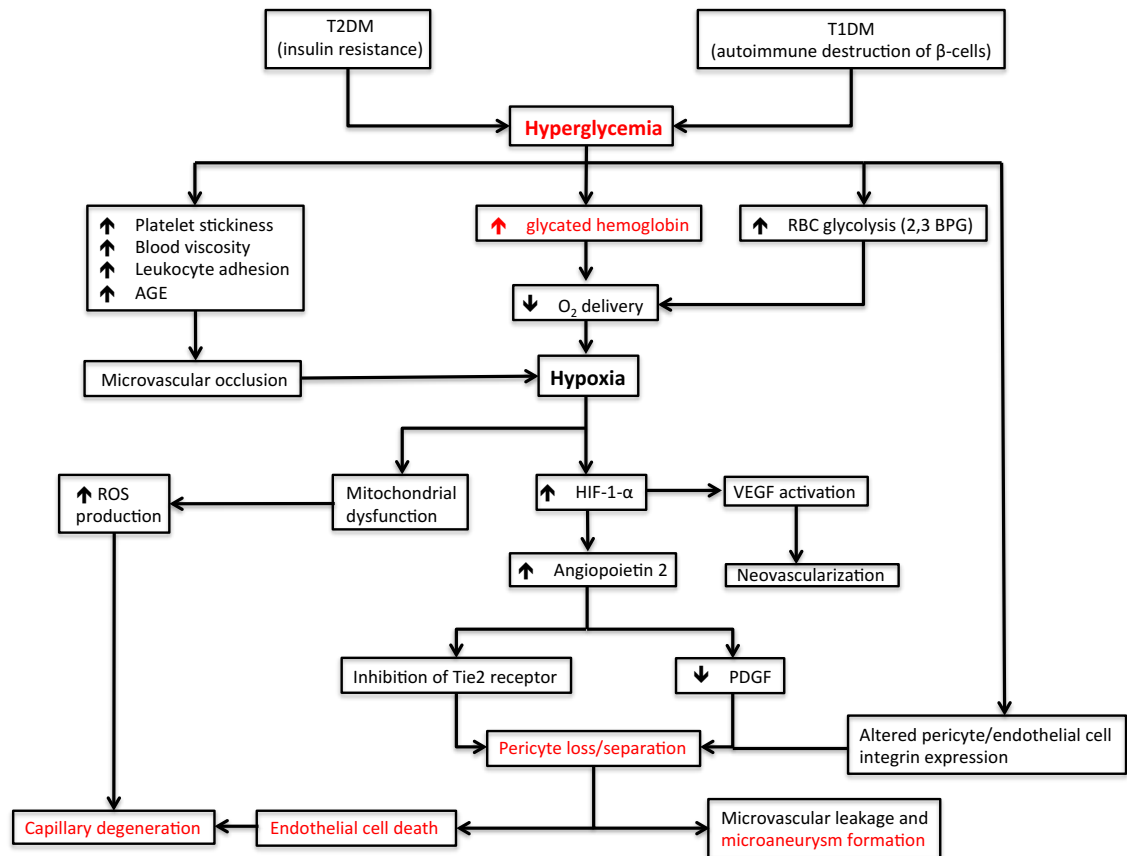


Figure 5.1: Proposed mechanism of hypoxia-induced pericyte loss.

Pericyte loss is one of earliest morphological changes seen in DR, however the exact mechanism is not fully understood. The proposed mechanism suggests an alternative pathway through which HG-induced changes may contribute to hypoxia and eventually pericyte loss. Text highlighted in red represents findings from the present study.

5.2B) In-vivo vascular integrity

Fluorescein angiography is routinely used to examine the inner retinal circulation of DR patients. FA allows for the detection of tortuous vessels, microaneurysms, microvascular leakage, microvascular occlusions and neovascularization. In the present study we were unable to conclusively determine whether or not microvascular leakage

was present due to the formation of cataracts that impeded clear imaging of the retina. Despite the obvious drawbacks of cataracts on retinal imaging, the formation of cataracts provides a unique opportunity to study the relationship between HG and early cataract development that is also seen in humans.

MA's are the first clinically detectable sign of DR. Although detection of MA's was limited by cataract formation, a single MA was found in an 18month HG retina. Hammes et al. 2002 describes an additional method for detecting MA formation in retinal digests. The present study found no evidence of any MA formation in retinal digests, however the retina in which the fundus MA was seen did not undergo retinal digestion. The lack of MA's seen in HG retinas, suggests 18-month-old NRs are in the early stages of DR that precede MA formation. Further aging or diet augmentation may be necessary to exacerbate the development of HG-related ocular changes.

Two distinct mechanisms are responsible for the formation of vascular networks: vasculogenesis and angiogenesis. Vasculogenesis refers to the development of new blood vessels when there are no pre-existing ones. Angiogenesis on the other hand, refers to the development of new blood vessels from pre-existing ones, such as neovascularization. The findings of the present study revealed an increased number of primary vessels with aging in HG retinas. Furthermore, this increase was primarily in smaller vessels, with a diameter between 10-20 μ m. These vessels were not tortuous and do not fit the classic traits of angiogenesis. This suggests that there is most likely not a change in absolute vessel number, but rather a change in vessel morphology. One possible explanation could be an increase in lumen diameter, which enables the vessels to be detected. Monique et al. 2011 reported increased retinal venular diameter in DR patients and also suggests this

as a risk factor for developing PDR. Further longitudinal investigation is necessary to confirm this progressive increase in vessel number associated with age and HG. Additionally, vitreal assessment of HIF and VEGF levels could determine if the environmental factors necessary for angiogenesis are present.

5.2C) Age-related dendritic sprouting

Current understanding of the pathogenesis of DR has evolved from a primarily vascular disorder to a neurovascular disease. Furthermore, emerging evidence suggests neuronal changes may precede the vascular abnormalities seen in DR. Amacrine cell dysfunction has been identified (by a loss of ERG OPs) as one of the earliest neuronal changes. Gastinger et al. 2006 reported a reduced number of cholinergic and dopaminergic amacrine cells in STZ rat retinas, which may contribute to decreased OP amplitudes seen in human DR. The present study similarly investigated amacrine cells and revealed age and HG-related changes in dopaminergic but not cholinergic amacrine cells. Control dopaminergic amacrine cells displayed age-related dendritic sprouting that was not present in age-matched HG retinas. In order to control for tangential sections, the thickness of the amacrine cell dendritic layer was normalized against both the INL and ONL. The difference found between the two subtypes of amacrine cells suggests HG may preferentially affect some but not all types of amacrine cells. It remains unclear whether these changes are sufficient to contribute to amacrine cell dysfunction, however future studies may consider investigating this relationship further. Liets et al. 2006 reported similar distinctions in cell-specific age-related sprouting of bipolar, but not horizontal or amacrine cells (cholinergic specifically). This evidence portrays the highly plastic and

adaptive capabilities of the retina, which may be hindered under harsh environments, such as HG. The results of the present study suggest HG may attenuate selective age-related sprouting that may extend to known sprouting cell-types (bipolar cells), however further investigation is required to clarify the effect of HG on retinal plasticity.

5.2D) Delayed dark-adaptation in diabetic retinopathy

It is well established that DR patients take longer to dark-adapt and also exhibit poor nighttime vision (Henson et al. 1979, Holfort et al. 2010). Dark adaptation is achieved through dopamine sensitive AII amacrine cell coupling of rod and cone bipolar cells. Specifically, Cx36 has been identified as the key gap junction that allows rod-driven signals to reach ON ganglion cells under scotopic conditions (Demb et al. 2002). Under photopic conditions, when dopamine levels are high, this pathway is blocked preventing transmission of any rod-based signals. The present study confirmed the presence of Cx36 in the OPL (presumably coupling photoreceptors) and IPL (presumably AII amacrine cells) and further revealed HG-induced down regulation in both layers. We suggest here that reduced Cx36 expression in the IPL may contribute to delayed dark adaptation times found in DR patients. Additionally, reduced Cx36 expression in the OPL may contribute to increased absolute scotopic thresholds and reduced nighttime vision. Although we do not understand the mechanism underlying Cx36 down regulation, it provides a feasible explanation for a common phenotype exhibited by DR patients.

5.3) Summary

The NR represents a novel animal model of diet-induced HG that displays many similarities to human DM. Although no animal model can perfectly recapitulate human pathology, a resemblance in major phenotypes should be present in order to allow for clinical translation. The slow time-course, increased adiposity and insulin resistance found in the NR closely resembles the natural progression of human T2DM and additionally provides a unique window for investigation. In particular, the cone-rich retina of the NR makes them an ideal candidate to undertake studies regarding the pathogenesis of DR.

HG NRs exhibited many classic hallmarks of human DR, such as pericyte loss, degeneration of capillaries and microaneurysm formation. Furthermore, conclusive determination of microvascular leakage was attenuated by the development of cataracts, which are often seen in human diabetic patients. In addition to the classic vascular changes associated with DR, HG NRs also displayed changes in inner retinal circuitry. This included a decreased ability for age-related dendritic sprouting specific to dopaminergic amacrine cells and also a marked reduction of Cx36 expression in the OPL and IPL. The results of this study demonstrate that NRs recapitulate the key pathological features of early human DR and provide a unique opportunity to study changes in the diabetic retina.

5.4) Future Directions

The findings of the current study show significant promise in using NRs to undertake studies regarding the development of HG and related ocular complications.

With a naturally progressing diet-induced HG that closely resembles human T2DM, the NR provides an invaluable opportunity to screen for genetic risk factors associated with developing T2DM. Recent evidence (Dean et al. 2004) suggests mutations in the *TCF7L2*, *ABCC8*, *CAPN10* and *HNF4A* genes are connected with a higher risk of developing T2DM. Molecular comparison between control and HG NRs could help to confirm or deny the involvement of these and other possible genes. Additionally, separation of HG NRs into early and late-onset groups could reveal novel findings about the impact of these genes on HG and DR progression. However, in order to effectively compare differences between these two groups, duration of HG rather than age will be the independent variable. This can be achieved through longitudinal FBG measurements (updated technique) collected biweekly to determine the time of HG-onset and also to further track any fluctuations in glycemia. This will provide valuable insight into the duration of HG associated with the early signs of DR.

The present study describes numerous anatomical differences between control and HG retinas (reduced age-related dendritic sprouting and Cx36 expression) that may contribute to functional deficits seen in human DR. However, due to initial difficulties with anesthesia, no functional assessments could be made. The introduction of a new inhalation anesthetic system offers an exciting opportunity to investigate ERG changes in relation to anatomy. Comparison between dark-adaptation time and Cx36 expression in the IPL would offer insight into the mechanism underlying delayed dark-adaptation in DR patients. Also, comparison of scotopic and photopic OP timing and amplitude as a function of HG and degree of age-related sprouting could help explain why amacrine

cells are preferentially affected in DR. Furthermore, the findings of Liets et al. 2006 (sprouting of bipolar cells) and Cuenca et al. 2005 (sprouting of bipolar and horizontal cell) suggest retinal plasticity is not limited to amacrine cells. Further, cross-sectional staining with PKC α (bipolar cells) and calbindin-D/parvalbumin (horizontal cells) would allow investigation of age-related sprouting in these cell types and also the effect of HG on retinal plasticity.

Cataracts are the leading cause of blindness worldwide and are currently only treated by surgical removal. A recent study (Zhao et al. 2015) introduced a novel potential treatment of cataracts through topical application of lanosterol (amphipathic molecule found within the lens). In vivo studies were performed on the cataracts of dogs; however further testing is required to determine the safety and efficacy of this new treatment. The HG-induced cataracts of the NR closely resemble human cataracts and offer a great opportunity to test this treatment on a wide range of cataract severities. Additionally, long-term effects on the retina could be assessed through ERG (retinal function) and post-mortem analysis (anatomy) in order to fully characterize the effect of this drug on the retina.

5.5) Conclusion

The present study demonstrates the suitability of the NR to undertake studies concerning the effect of HG on the retina. The presence of key pathological features (pericyte loss, degeneration of capillaries, microaneurysm formation) and slow time course makes the NR a valuable source of new understanding about the mechanism of DR and also a potential candidate to undergo novel therapies. Results from the study

revealed novel findings about the effect of HG on retinal plasticity and also presented a possible role of hypoxia in pericyte loss. Clinical translation of these findings is supported by a high degree of similarity between the complex retinal circuitry of humans and NRs. Lastly, the spontaneous development of HG offers a rare chance to screen for genetic polymorphisms associated with T2DM and related complications. Taken together, the NR provides a unique opportunity to study the pathogenesis of DM and associated complications.

References

Aiello, S. E. Bursell, A. Clermont et al. Vascular endothelial growth factor-induced retinal permeability is Experimental Diabetes Research mediated by protein kinase C in vivo and suppressed by an orally effective β -isoform-selective inhibitor. *Diabetes*. 1997; vol. 46; no. 9: 1473–1480.

Allt G, Lawrenson JG. Pericytes: cell biology and pathology. *Cells Tissues Organs*. 2001; 169:1–11.

American Diabetes Association. (2007). National diabetes statistics report.

American Foundation for the Blind. September 2008

Arden GB, Wolf JE, Collier J, Wolff C, Rosenberg M. Dark adaptation is impaired in diabetic before photopic loss can be seen. Can hypoxia contribute to diabetic retinopathy? Hollyfield JG (ed). *Retinal Degenerative Diseases and Experimental Therapy*. 1999; 305-325.

Armulik, A., Abramsson, A., & Betsholtz, C. Endothelial/pericyte interactions. *Circulation Research* 2005; 97: 512–23.

Blanchong, J. A., McElhinny, T. L., Mahoney, M. M., and Smale, L. Nocturnal and diurnal rhythms in the unstriped Nile rat, *Arvicanthis niloticus*. *J. Biol. Rhythms*. 1999; 14: 364–377.

Bobbie, M.W., Roy, S., Trudeau, K., Munger, S.J. & Simon, A.M. Reduced connexin 43 expression and its effect on the development of vascular lesions in retinas of diabetic mice. *Invest. Ophthalmol. Vis. Sci*. 2010; 51: 3758–3763.

Bobu, C., Craft, C. M., Masson-Pevet, M., and Hicks, D. Photoreceptor organization and rhythmic phagocytosis in the Nile rat *Arvicanthis ansorgei*: a novel

diurnal rodent model for the study of cone pathophysiology. *Invest. Ophthalmol. Vis. Sci.* 2006; 47: 3109–3118

Candelario-Jalil, E., Yang, Y. & Rosenberg, G.A. Diverse roles of matrix metalloproteinases and tissue inhibitors of metalloproteinases in neuroinflammation and cerebral ischemia. *Neuroscience.* 2009; 158: 983–994.

Chaabo, F., Pronczuk, A., Maslova, E., & Hayes, K. Nutritional correlates and dynamics of diabetes in the Nile rat (*Arvicanthis niloticus*): a novel model for diet-induced type 2 diabetes and the metabolic syndrome. *Nutrition & Metabolism.* 2010; 7; 29: 1743-7075-7-29

Cheng, Y. J., Gregg, E. W., Geiss, L. S., Imperatore, G., Williams, D. E., Zhang, X., Saaddine, J. B. Association of A1C and fasting plasma glucose levels with diabetic retinopathy prevalence in the U.S. population: Implications for diabetes diagnostic thresholds. *Diabetes Care.* 2009; 32(11): 2027–2032.

Cheung, A. K., Fung, M. K., Lo, A. C., Lam, T. T., So, K. F., Chung, S. S. and Chung, S. K. Aldose reductase deficiency prevents diabetes-induced blood-retinal barrier breakdown, apoptosis, and glial reactivation in the retina of db/db mice. *Diabetes.* 2005; 54: 3119-3125.

Cogan D, Diabetic, I. V. *Retinal Patterns.* Public Health. 1879.

Cuenca N, Pinilla I, Sauvé Y, Lund R. Early changes in synaptic connectivity following progressive photoreceptor degeneration in RCS rats. *European Journal of Neuroscience.* 2005; Volume 22, Issue 5, pages 1057–1072.

Danaei G, Finucane MM, Lu Y, Singh GM, Cowan MJ, Paciorek CJ, Lin JK, Farzadfar F, Khang YH, Stevens GA, Rao M, Ali MK, Riley LM, Robinson CA, Ezzati M, on behalf of the Global Burden of Metabolic Risk Factors of Chronic Diseases Collaborating Group (Blood Glucose). National, regional, and global trends in fasting plasma glucose and diabetes prevalence since 1980: systematic analysis of health examination surveys and epidemiological studies with 370 country-years and 2.7 million participants. *The Lancet*. 2011;378: 331-40.

The Diabetes Control and Complications Trial (DCCT). The effect of intensive treatment of diabetes on the development and progression of long-term complications in insulin-dependent diabetes mellitus. The Diabetes Control and Complications Trial Research Group. *New Engl J Med*. 1993; 329: 977–986.

Dean L, McEntyre J. The Genetic Landscape of Diabetes [Internet]. Bethesda (MD): National Center for Biotechnology Information (US); 2004. Chapter 3, Genetic Factors in Type 2 Diabetes. 2004 Jul 7.

Delany MJ and Kansiimeruhanga WDK. Observations of the ecology of rodents from a small arable plot near Kampala, Uganda. *Rev Zool Bot Afr*. 1970; 81: 417-425

Demb, J. B., & Pugh, E. N. Connexin 36 forms synapses essential for night vision. *Neuron*. 2002; 36: 551–553.

Diabetes February 1989 38:2 159-163.

Dietrich, N., & Hammes, H. *Animal Models in Diabetes Research*. 2012; 933: 291–302.

Fowler, M. J. *Microvascular and Macrovascular Complications of Diabetes*. 2008; 26(2): 77–82.

Frank R. N., "Diabetic retinopathy," *New England Journal of Medicine*. 2004; vol. 350, no. 1, pp. 48–58.

Gaillard F, Bonfield S, Gilmour GS, Kuny S, Mema SC, Martin BT, Smale L, Crowder N, Stell WK, Sauvé Y. Retinal anatomy and visual performance in a diurnal cone-rich laboratory rodent, the Nile grass rat (*Arvicanthis niloticus*). *J Comp Neurol*. 2008; 510: 525-538.

Gaillard F, Kuny S, Sauvé Y. Topographic arrangement of S-cone photoreceptors in the retina of the diurnal Nile grass rat (*Arvicanthis niloticus*). *Invest Ophthalmol Vis Sci*. 2009; 50: 5426- 5434.

Gastinger, M. J., Kunselman, A. R., Conboy, E. E., Bronson, S. K. and Barber, A. J. Dendrite remodeling and other abnormalities in the retinal ganglion cells of *Ins2Akita* diabetic mice. *Invest. Ophthalmol. Vis. Sci*. 2008; 49: 2635-2642.

Gastinger, M. J., Singh, R. S. J., & Barber, A. J. Loss of cholinergic and dopaminergic amacrine cells in streptozotocin-diabetic rat and *Ins2Akita*-diabetic mouse retinas. *Investigative Ophthalmology & Visual Science*. 2006; 47(7): 3143–50.

Gerhardt, H., Wolburg, H. & Redies, C. N-cadherin mediates pericytic-endothelial interaction during brain angiogenesis in the chicken. *Dev. Dyn*. 2000; 218: 472–479.

Gilmour G.S., Gaillard F., Watson J., Kuny S., Mema SC, Bonfield S, Stell WK, Sauvé Y. The electroretinogram (ERG) of a diurnal cone-rich laboratory rodent, the Nile grass rat (*Arvicanthis niloticus*). *Vis Res*. 2008; 8: 2723-2731

Hamilton, N.B., Attwell, D. & Hall, C.N. Pericyte-mediated regulation of capillary diameter: a component of neurovascular coupling in health and disease. *Front. Neuroenergetics*. 2010; 2, 5: 81.

Hammes HP, Porta M. Experimental Approaches to Diabetic Retinopathy. *Frontiers in Diabetes*. 2010; Vol. 20

Hammes HP, Lin J, Renner O, Shani M, Lundqvist A, Betsholtz C, Brownlee M, Deutsch U: Pericytes and the pathogenesis of diabetic retinopathy. *Diabetes*. 2002; 51: 3107–3112.

Hammes, B. Wellensiek, I. Klöting, E. Sickel, R. G. Bretzel, and M. Brownlee, “The relationship of glycaemic level to advanced glycation end-product (AGE) accumulation and retinal pathology in the spontaneous diabetic hamster,” *Diabetologia*. 1998; vol. 41, no. 2, pp. 165–170.

Hammes, H.P. et al. Angiopoietin-2 causes pericyte dropout in the normal retina: evidence for involvement in diabetic retinopathy. *Diabetes*. 2004; 53: 1104–1110.

Hellström, M. et al. Lack of pericytes leads to endothelial hyperplasia and abnormal vascular morphogenesis. *J. Cell Biol.* 2001; 153: 543–553.

Henson, D. B., & North, R. V. Dark adaptation in diabetes mellitus. *The British Journal of Ophthalmology*. 1979; 63(8): 539–541.

Hofmann, J.J. & Iruela-Arispe, M.L. Notch signaling in blood vessels: who is talking to whom about what? *Circ. Res.* 2007; 100: 1556–1568.

Holfort, S. K., Jackson, G. R., & Larsen, M. Dark adaptation during transient hyperglycemia in type 2 diabetes. *Experimental Eye Research*. 2010; 91(5): 710–714.

Holopigian, K., Seiple, W., Lorenzo, M., & Carr, R. A Comparison of Photopic and Scotopic Electroretinographic Changes in Early Diabetic Retinopathy. *Investigative Ophthalmology*. 1992; 33(10): 2773–2780.

<http://jaxmice.jax.org/>; accessed on 7-Aug-2015

<http://www.diacomp.org>; accessed on 5-Aug-2015.

<https://nei.nih.gov/health/diabetic/retinopathy>; accessed on 9-Aug-2015

Hughes, J. M., Brink, A., Witmer, A. N., Hanraads-de Riemer, M., Klaassen, I., and Schlingemann, R. O. Vascular leucocyte adhesion molecules unaltered in the human retina in diabetes. *Br. J. Ophthalmol.* 2004; 88: 566–572 20.

Hughes, S., Gardiner, T., Hu, P., Baxter, L., Rosinova, E., & Chan-Ling, T. Altered pericyte-endothelial relations in the rat retina during aging: Implications for vessel stability. *Neurobiology of Aging*. 2006; 27(12): 1838–1847.

Hummel K. P., M.M. Dickie, and D.L. Coleman, “Diabetes, a new mutation in the mouse,” *Science*. 1966; vol.153, no. 3740, pp. 1127– 1128.

Iglesias, P., & Díez, J. J. Management of endocrine disease: A clinical update on tumor-induced hypoglycemia. *European Journal of Endocrinology*. 2014; 170(4).

Jeganathan, V. S. E., Wang, J. J., & Wong, T. Y. Ocular associations of diabetes other than diabetic retinopathy. *Diabetes Care*. 2008; 31(9): 1905–1912.

Josifova, T., Plestina-Borjan, I., & Henrich, P. B. Proliferative diabetic retinopathy: Predictive and preventive measures at hypoxia induced retinal changes. *EPMA Journal*. 2010; 1(1): 73–77.

Katona C, Smale L. Wheel-running rhythms in *Arvicanthis niloticus*. *Physiology & Behavior*. 1997; 61: 365-372.

Katz, G., Levkovitch-Verbin, H., Treister, G., Belkin, M., Ilany, J., & Polat, U. Mesopic foveal contrast sensitivity is impaired in diabetic patients without retinopathy. *Graefe's Archive for Clinical and Experimental Ophthalmology*. 2010; 248(12): 1699–1703.

Kim, S. Y., Johnson, M. A., McLeod, D. S., Alexander, T., Otsuji, T., Steidl, S. M., Hansen, B. C. and Lutty, G. A. Retinopathy in monkeys with spontaneous type 2 diabetes. *Invest. Ophthalmol. Vis. Sci.* 2004; 45: 4543-4553.

Klein BE, Klein R, Moss SE. Incidence of cataract surgery in the Wisconsin Epidemiologic Study of Diabetic Retinopathy. *Am J Ophthalmol*. 1995;119: 295–300.

Klein BE, Klein R, Wang Q, Moss SE. Older-onset diabetes and lens opacities. The Beaver Dam Eye Study. *Ophthalm Epidemiol*. 1995; 2: 49–55.

Klein, B.E. K. Klein, S.E. Moss, and K.J. Cruickshanks, "The Wisconsin epidemiologic study of diabetic retinopathy XV: the long-term incidence of macular edema," *Ophthalmology*. 1995; vol. 102, no. 1, pp. 7–16.

Kryger Z, Galli-Resta L, Jacobs GH, Reese BE. The topography of rod and cone photoreceptors in the retina of the ground squirrel. *Visual Neuroscience*. 1998; 15: 685-691.

Kuroki, E. E. Voest, S. Amano et al., "Reactive oxygen intermediates increase vascular endothelial growth factor expression in vitro and in vivo," *Journal of Clinical Investigation*. 1996; vol. 98, no. 7, pp. 1667–1675.

Lai, A. K. W., & Lo, A. C. Y. Animal models of diabetic retinopathy: summary and comparison. *Journal of Diabetes Research*. 2013; 106-594.

Le May, C., Chu, K., Hu, M., Ortega, C. S., Simpson, E. R., Korach, K. S., ... Mauvais-Jarvis, F. Estrogens protect pancreatic beta-cells from apoptosis and prevent insulin-deficient diabetes mellitus in mice. *Proceedings of the National Academy of Sciences of the United States of America*. 2006; 103(24): 9232–9237.

Liets, L. C., Eliasieh, K., van der List, D. a, & Chalupa, L. M. Dendrites of rod bipolar cells sprout in normal aging retina. *Proceedings of the National Academy of Sciences of the United States of America*. 2006; 103(32): 12156–60.

Lindhahl, P., Johansson, B.R., Leveen, P. & Betsholtz, C. Pericyte loss and microaneurysm formation in PDGF-B-deficient mice. *Science*. 1997; 277: 242–245.

Ma RC, Tong PC. Epidemiology of type 2 diabetes. In *The Textbook of Diabetes*. 4th ed. Holt RI, Cockram C, Flyvbjerg A, Goldstein BJ, Eds. Chichester, UK, Blackwell Publishing. 2010.

Martin, P. M., Roon, P., Van Ells, T. K., Ganapathy, V. and Smith, S. B. Death of retinal neurons in streptozotocin-induced diabetic mice. *Invest. Ophthalmol. Vis. Sci*. 2004; 45: 3330-3336.

Matthews D. R., I. M. Stratton, S. J. Aldington, R. R. Holman, and E. M. Kohner, “Risks of progression of retinopathy and vision loss related to tight blood pressure control in type 2 diabetes mellitus: UKPDS 69,” *Archives of Ophthalmology*. 2004; vol. 122, no. 11, pp. 1631–1640.

McLeod, D. S., Lefer, D. J., Merges, C., and Luty, G. A. Enhanced expression of intracellular adhesion molecule-1 and P-selectin in the diabetic human retina and choroid. *Am. J. Pathol*. 1995; 147: 642–653 19.

Miyamoto, K., Hiroshiba, N., Tsujikawa, A., and Ogura, Y. In vivo demonstration of increased leukocyte entrapment in retinal microcirculation of diabetic rats. *Invest. Ophthalmol. Vis. Sci.* 1998; 39: 2190–2194.

Miyamoto, K., Khosrof, S., Bursell, S. E., Rohan, R., Murata, T., Clermont, A. C., Aiello, L. P., Ogura, Y., and Adamis, A. P. Prevention of leukostasis and vascular leakage in streptozotocin-induced diabetic retinopathy via intercellular adhesion molecule-1 inhibition. *Proc. Natl. Acad. Sci. U. S. A.* 1999; 96: 10836–10841.

Mizutani M, Kern TS, Lorenzi M: Accelerated death of retinal microvascular cells in human and experimental diabetic retinopathy. *J Clin Invest* 1996; 97: 2883–2890.

Movasat, M., Modarresi, M., Mansouri, M., Nili-ahmadabadi, M., & Rajabi, M. Oscillatory Potentials in Diabetic Retina without Retinopathy. 2008; 20(1).

Monique S. Roy, MD; Ronald Klein, MD; Malvin N. Janal. Retinal Venular Diameter as an Early Indicator of Progression to Proliferative Diabetic Retinopathy With and Without High-Risk Characteristics in African Americans With Type 1 Diabetes Mellitus. *Arch Ophthalmol.* 2011; 129(1): 8-15.

Müller, B., & Peichl L. Topography of cones and rods in the tree shrew retina. *Journal of Comparative Neurology.* 1989; 282: 581-594.

Noda, K., Melhorn, M. I., Zandi, S., Frimmel, S., Tayyari, F., Hisatomi, T., ... Hafezi-Moghadam, A. An animal model of spontaneous metabolic syndrome: Nile grass rat. *FASEB Journal : Official Publication of the Federation of American Societies for Experimental Biology.* 2010; 24(7): 2443–53.

Noda, K., Nakao, S., Zandi, S., Sun, D., Hayes, K. C., & Hafezi-Moghadam, A. Retinopathy in a novel model of metabolic syndrome and type 2 diabetes: new insight on

the inflammatory paradigm. *FASEB Journal : Official Publication of the Federation of American Societies for Experimental Biology*. 2014; 28(5): 2038–46.

Nguyen, T. T., and Wong, T. Y. Retinal vascular changes and diabetic retinopathy. *Curr. Diab. Rep.* 2009; 9: 277–283.

Park, S. W., Yun, J.-H., Kim, J. H., Kim, K.-W., Cho, C.-H., & Kim, J. H. Angiopoietin 2 Induces Pericyte Apoptosis via $\alpha 3\beta 1$ Integrin Signaling in Diabetic Retinopathy. *Diabetes*. 2014; 63: 3057–3068.

Peichl L., & Gonzalez-Soriano, J. Morphological types of horizontal cell in rodent retinae: a comparison of rat, mouse, gerbil and guinea pig. *Visual Neuroscience*. 1994; 11: 501-517.

Public Health Agency of Canada. Public Health Agency of Canada Steering Committee on Health-Adjusted Life Expectancy. Health-Adjusted Life Expectancy in Canada: 2010 Report by the Public Health Agency of Canada. In press. Ottawa. 2011.

Qian, H., & Ripps, H. Neurovascular interaction and the pathophysiology of diabetic retinopathy. *Experimental Diabetes Research*. 2011.

Reznicek L, Kernt M, Haritoglou C, Ulbig M, Kampik A, Neubauer AS. Correlation of leaking microaneurysms with retinal thickening in diabetic retinopathy. *International Journal of Ophthalmology*. 2011; 4(3): 269-271.

Robinson, R., Barathi, V. a, Chaurasia, S. S., Wong, T. Y., & Kern, T. S. Update on animal models of diabetic retinopathy: from molecular approaches to mice and higher mammals. *Disease Models & Mechanisms*. 2012; 5(4): 444–56.

Robison Jr., M. Nagata, T. N. Tillis, N. Laver, and J. H. Kinoshita, "Aldose reductase and pericyte-endothelial cell contacts in retina and optic nerve," *Investigative Ophthalmology and Visual Science*. 1989; vol. 30, no. 11, pp. 2293–2299.

Rossi, G. Diagnosis and classification of diabetes mellitus. *Recenti Progressi in Medicina*. 2004; 101(7-8): 274–276.

Ruth A Kava, David B West, Valerie A Lukasik, and M R C Greenwood. Sexual Dimorphism of Hyperglycemia and Glucose Tolerance in Wistar Fatty Rats. 1989.

Saharinen, P. et al. Angiopoietins assemble distinct Tie2 signaling complexes in endothelial cell-cell and cell-matrix contacts. *Nat. Cell Biol*. 2008; 10: 527–537.

Saïdi T, Mbarek S, Omri S, Behar-Cohen F, Chaouacha-Chekir RB, Hicks D. The sand rat, *Psammomys obesus*, develops type 2 diabetic retinopathy similar to humans. *Invest Ophthalmol Vis Sci*. 2011; 52: 8993-9004.

Shepro D, Morel NML. Pericyte physiology. *FASEB J*. 1993; 7: 1031–1038.

Shuboni, D. D., Cramm, S., Yan, L., Nunez, a. a., & Smale, L. Acute Behavioral Responses to Light and Darkness in Nocturnal *Mus musculus* and Diurnal *Arvicantis niloticus*. *Journal of Biological Rhythms*. 2012; 27(4): 299–307.

Sims DE. The pericyte—a review. *Tissue Cell*. 1986; 18: 153–174.

Solheim, T. S., Blum, D., Fayers, P. M., Hjerstad, M. J., Stene, G. B., Strasser, F., & Kaasa, S. Weight loss, appetite loss and food intake in cancer patients with cancer cachexia: three peas in a pod? - analysis from a multicenter cross sectional study. *Acta Oncologica*. 2014; 53(4): 539–46.

Stratton, I. M., Adler, a I., Neil, H. a, Matthews, D. R., Manley, S. E., Cull, C. a, Holman, R. R. Association of glycaemia with macrovascular and microvascular complications of type 2 diabetes (UKPDS 35): prospective observational study. *BMJ (Clinical Research Ed.)*, 2000; 321(7258): 405–412.

Taylor, P. D., Wickenden, A. D., Mirrlees, D. J., and Poston, L. Endothelial function in the isolated perfused mesentery and aortae of rats with streptozotocin-induced diabetes: effect of treatment with the aldose reductase inhibitor, ponalrestat. *Br. J. Pharmacol.* 1994; 111: 42–48.

Thylefors B, Negrel A D, Pararajasegaram R, Dadzie K Y. Global data on blindness. *Bull World Health Organ.* 1995; 73: 115–121.

Tilton R.G., Kilo C. and Williamson J.R. Pericyte- endothelial relationships in cardiac and skeletal muscle capillaries. *Microvasc. Res.* 1979; 18: 325-335.

Tzekov, R., & Arden, G. B. The electroretinogram in diabetic retinopathy. *Survey of Ophthalmology.* 1999; 44(1): 53–60.

Vijan S. Type 2 Diabetes. *Ann Intern Med.* 2010; 152: 3-1.

Viswanath, K., & McGavin, M. Diabetic Retinopathy : Clinical Findings and Management Diabetic Retinopathy. *Community Eye Health.* 2003; 16(46): 21–24.

Walshe, T.E. et al. TGF-beta is required for vascular barrier function, endothelial survival and homeostasis of the adult microvasculature. *PLoS ONE* 4. 2009.

Wang J, Takeuchi T, Tanaka S, Kubo SK, Kayo T, Lu D, Takata K, Koizumi A, Izumi T. A mutation in the insulin 2 gene induces diabetes with severe pancreatic beta-cell dysfunction in the Mody mouse. *J Clin Invest.* 1999; 103(1): 27-37.

Weir, G. C., & Bonner-Weir, S. Five Stages of Evolving Dysfunction During Progression to Diabetes. *Diabetes*. 2004; 53(3): S16–21.

Winkler, E. a, Bell, R. D., & Zlokovic, B. V. Central nervous system pericytes in health and disease. *Nature Neuroscience*. 2011; 1398–1405.

World Health Organization. Abbreviated Report of a WHO Consultation. Geneva: WHO;. Use of Glycated Haemoglobin (HbA1c) in the Diagnosis of Diabetes Mellitus. 2011.

www.cdc.gov/diabetes

<http://diabetesdigest.com/living-with-type-2-diabetes-progression/>. Natural Progression of Type 2 Diabetes. February 7. 2014

Zhao, L., Chen, X.-J., Zhu, J., Xi, Y.-B., Yang, X., Hu, L.-D., ... Zhang, K. Lanosterol reverses protein aggregation in cataracts. *Nature*. 2015.